Surface Mixing Layers in the Sargasso Sea

A. E. GARGETT

Institute of Ocean Sciences, Patricia Bay, Sidney, B.C., Canada V8L 4B2

T. B. SANFORD

Woods Hole Oceanographic Institution, Woods Hole MA 02543

T. R. OSBORN

Institute of Oceanography, University of British Columbia, Vancouver, B.C. V6T 1W5

(Manuscript received 28 August 1978, in final form 19 June 1979)

ABSTRACT

Observations of turbulent energy dissipation rate ϵ in the deep surface mixed layer at a mid-Sargasso site are presented: two occupations of this site include a large range of local meteorological forcing. Two frontal passages and a large time interval between profiles during the first series of measurements preclude examination of the turbulent kinetic energy balance: qualitatively, a profile taken during the strongest wind-wave forcing of the observation set suggests that layer deepening was not being driven directly from the surface, but by a shear instability at the mixed layer base. A quantitative assessment of terms in the steady-state locally balanced model of the turbulent kinetic energy budget proposed by Niiler (1975) has been possible for two profiles having dissipation characteristics and surface meteorological conditions which allow us to argue for the absence of all but a few of the possible source/sink terms in the turbulent kinetic energy balance. In one case, a steady-state local balance is possible. In the other case, a local balance can be maintained by giving up the steady-state assumption, i.e., by including the time rate of decay of the turbulent kinetic energy. Other possible balances exist. The analysis of the surface mixed-layer turbulent kinetic energy balance highlights two major uncertainties—parameterization of the wind-wave forcing term and lack of reliable dissipation measurements in the upper 10–20 m of the water column.

1. Introduction

Recent years have seen a proliferation of ocean surface mixed-layer models, spurred by the need for coupled ocean-atmosphere models in long-range weather prediction and studies of climate dynamics. Most models presently proposed for the surface mixed layer assume that the ocean is horizontally homogeneous, and assume that the relevant dynamics are local in character, i.e., the depth and heat content of the mixed layer primarily result from local surface atmospheric forcing. If correct, this assumption of local response allows highly desirable decoupling of the short-term behavior of the surface layer from unknown changes in properties of the deeper layers of the ocean. In addition, most surface layer models are integrated models; the governing equations are simplified, and resulting computations shortened, by vertical integration from the surface to the base of the mixed layer. The class of integrated models involves the additional assumption that the bulk of the mixed layer moves as a slab; and that mean horizontal velocity U as well as density is constant throughout the layer, except for thin regions near the ocean surface and at the base of the surface mixed layer (SML). Specific models differ in proposed mechanisms by which energy from the surface wind field increases both the kinetic and potential energies of the SML as it deepens during periods of active atmospheric forcing. Kraus and Turner (1967) and Denman (1973) explored a model (referred to as DKT) in which turbulent kinetic energy is produced in the region of wave-induced mean shear at the ocean surface. Pollard *et al.* (1973) (PRT) considered an alternate zone of production of turbulent kinetic energy in the mean shear at the base of the mixed layer. In this model, the postulated mean motion is the inertial oscillation of the slablike mixed layer, shown by Pollard (1970) and Pollard and Millard (1970) to be associated with sudden changes in surface wind field. Niiler (1975) has produced a composite slab model which incorporates both of these mechanisms, as well as possible forcing by an unstable buoyancy flux at the ocean surface, into a turbulent kinetic energy equation. Observational data used to test such models have generally come from Ocean Weather Stations, in particular, Stations P (50°N, 145°W) and N (30°N, 140°W), both located

0022-3670/79/061090-22$09.50

in mid-gyre regions of the eastern North Pacific (Denman and Miyake, 1973; Thompson, 1976).

The only exception to the integrated models is the work of Mellor and Durbin (1975), who replace the turbulent Reynolds stresses and heat flux in mean flow momentum and heat equations, using a rather complex eddy viscosity/diffusivity model with three empirical constants determined from neutral turbulent flow observations. With an impulsively applied surface wind stress, the model was used to calculate mixed-layer deepening and the set-up of the velocity field in the mixed layer. Instantaneous temperature profiles often show a steplike feature at the mixed-layer base, while the velocity field undergoes strong inertial oscillations. There is substantial vertical mean shear, so that the mixed layer cannot be treated as a slab during active wind forcing. However, with cessation of the wind, the model shows adjustment to slab flow within an extremely short time, less than one-fifth of an inertial period: the authors also state that turbulence within the surface layer becomes negligible within the same time period. Predictions of this model agree remarkably well with the isotherm contours observed at Station P by Denman and Miyake (1973); we note, however, that this agreement was obtained using a drag coefficient (in the standard expression deriving surface wind stress from observed wind speed at 10 m) of 0.002, 50% larger than the value of 0.0013 used by Denman and Miyake (1973).

In this paper, we present two sets of upper ocean profiles of turbulent energy dissipation and mean velocity from a site in the Sargasso Sea (35°N, 66° 30′W. The two observation periods were part of FAME, the Fine and Microstructure Experiment (Sanford and Hogg, 1977) of October–November 1975. This was not planned as a SML experiment, and meteorological measurements were confined to standard shipboard observations every 4 h. Since the first 6-day observation period included one atmospheric frontal passage and was preceded by another, our rudimentary meteorological observations and the erratic timing of dissipation profiles make it impossible to examine the dynamics of mixed-layer response during this period. We present these dissipation profiles as an addition to the sparse literature (Grant *et al.*, 1968; Osborn, 1978) of direct measurements of turbulent kinetic energy dissipation rate in the ocean surface mixed layer during and after a period of active wind forcing, and comment on certain features of the profiles in the context of assumptions and predictions of various theoretical models. During a 24 h re-occupation of the same site two weeks later, more stable meteorological conditions coupled with features of the observed time series of mean shear and density, and turbulent dissipation allow an examination of the turbulent kinetic energy balance around the time of the final dissipation profile, within a framework provided by Niiler's (1975) composite slab model.

2. The profile measurements

a. Dissipation profiles

The dissipation profiles were taken with CAMEL, the free-fall vehicle built and described by Osborn (1977). The sensing element for vertical shear of horizontal velocity on vertical scales of ~4–50 cm is an airfoil probe originally developed by Osborn and Siddon (1975). Calibration techniques and present knowledge of probe performance have recently been documented by Osborn and Crawford (1977). Probes used in FAME have two orthogonal sensing elements, giving two independent estimates of small-scale shear assuming horizontal homogeneity on the microscale. Standard processing divides the output from a shear channel into roughly 2.5 db intervals on the basis of the signal from a Vibrotron pressure transducer. For each such interval, the one-sided power spectrum is formed and its integral calculated over the frequency range of 0.59 to 18.5 Hz, corresponding to a wavenumber range of roughly 0.01–0.4 cpm for the 40–50 cm s^{-1} fallspeeds typical of CAMEL. The measured shear variance is then converted to an estimate for ϵ, the dissipation rate of turbulent energy, by multiplying by (15/2) ν, where ν is the kinematic viscosity of seawater (Miyake and Koizumi, 1948). If ϕ_c is the power spectral density of a cross-stream component of the turbulent velocity (the shear probe is a cross-flow sensor), then

$$\epsilon = (15/2)\nu \int_0^\infty k^2 \phi_c dk \approx (15/2)\nu \int_{K_L}^{k_U} \phi_s dk,$$

where ϕ_s is the power spectral density of the shear and (k_L, k_U) the finite wavenumber range of the integration. The accuracy of this estimate depends on three major factors: the assumption of isotropy, the accuracy of the measured shear spectrum ϕ_s, and the degree to which the interval $k_L \leq k \leq k_U$ contains a major part of the variance of the shear field. The isotropy assumption, which makes it possible to express ϵ as the above function of only one component of the fluctuating velocity, ought to be acceptable in the SML, if anywhere in the ocean. Indeed, in discussion of the second set of observations (Section 4), we present some indirect evidence of small-scale isotropy. Below the SML this assumption is used by default for lack of information on the degree of anisotropy to be expected in the stably stratified regions of the ocean. Values of ϵ may be converted to rms shear (in units of s^{-2}) by dividing by 7.5ν, where ν ranges from 0.014 to 0.0094 cm^2 s^{-1} for the range of temperature (10–26°C) encountered during the cruise. The absolute error intro-

duced into the measurement by possible calibration errors has been assessed by Crawford (1976) and is ~50% for fallspeeds of 40–50 cm s^{-1}. However, the absolute error of measurement is often of less concern than relative error, which is chiefly determined by the last factor mentioned above, the fraction of the shear variance contained in the restricted wavenumber range $k_L \leq k \leq k_U$ over which the shear spectra are integrated. On the basis of variance-conserving plots of individual shear spectra, such as those shown in Fig. 1, we estimate that the fraction of the total variance included in the fixed integration range varies from ~1.0 for $\epsilon = 10^{-4.5}$ cm^2 s^{-3}, ~0.9 for $\epsilon = 10^{-3}$ cm^2 s^{-3} to ~0.8 for $\epsilon = 10^{-2}$ cm^2 s^{-3}. Thus the relative values of ϵ have an uncertainty of perhaps 20%, with the highest values being underestimated by use of a fixed integration range.

One of the problems with the shear sensor used in the vertical profiling mode has been a temperature sensitivity of the bimorph beams used to sense side-force pressures caused by fluctuating velocities. When the probe passes through strong finestructure-scale vertical temperature gradients, this sensitivity causes a mean offset which decays with time. An example of this effect appears in Fig. 2 just below 65 m depth, at the quiescent base of a mixed layer observed ~60 km northeast of Bermuda. This low-frequency offset is not accompanied by high-frequency contamination of the shear signals, and when present in an analysis block, is generally confined to the lowest spectral estimate, which is not used in the integral for ϵ. Because the time scale of the temperature response of the beam is much longer than that of the finestructure temperature feature which initiates it (due to the thermal inertia of the epoxy in which the beams are set), we expect no contamination from microscale temperature fluctuations, since these are associated with much higher effective frequencies than finestructure. Crawford and Osborn (1979, Fig. 6) present an example from the equatorial Atlantic, in which both shear components, indeed, remain at noise level through a region of microscale fluctuations of the temperature gradient. Moreover, since the temperature sensitivity of individual beams varies considerably and each probe carries two beams, one can often choose the channel with the smaller temperature effect in regions of finestructure temperature gradients. For the observations considered in this paper, data loss through the temperature effect was small, confined to occasional regions of very large temperature gradient at the base of the SML. Contaminated measurements have been removed manually from any of the dissipation profiles shown. A more serious data loss arose through contamination of near-surface values by low-frequency oscillations, which fortunately decayed rather rapidly with depth (examples of this effect appears in the analogue shear traces of Figs. 2 and 4). The oscillations may be caused by tube wobble originating during launch, or by true side-force pressures associated with the velocity field of surface swell. Whatever the origin, the low-frequency contamination appears in the standard dissipation profiles as unusually large dif-

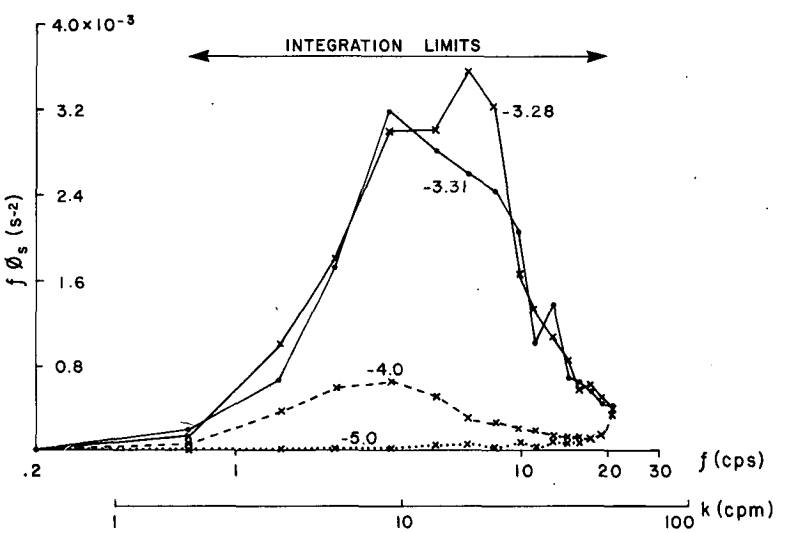

FIG. 1. Variance-preserving plots of velocity shear spectra for various signal strengths. For isotropic turbulence, the rate of turbulent energy dissipation ϵ is proportional to the integral under this curve, and the individual curves are labeled with the value of logϵ derived in this way.

A two-axis airfoil probe was used, giving two independent estimates of the shear spectrum for each section of record. The spectra from both channels are shown (×) shear 1, (•) shear 2 for one of the records.

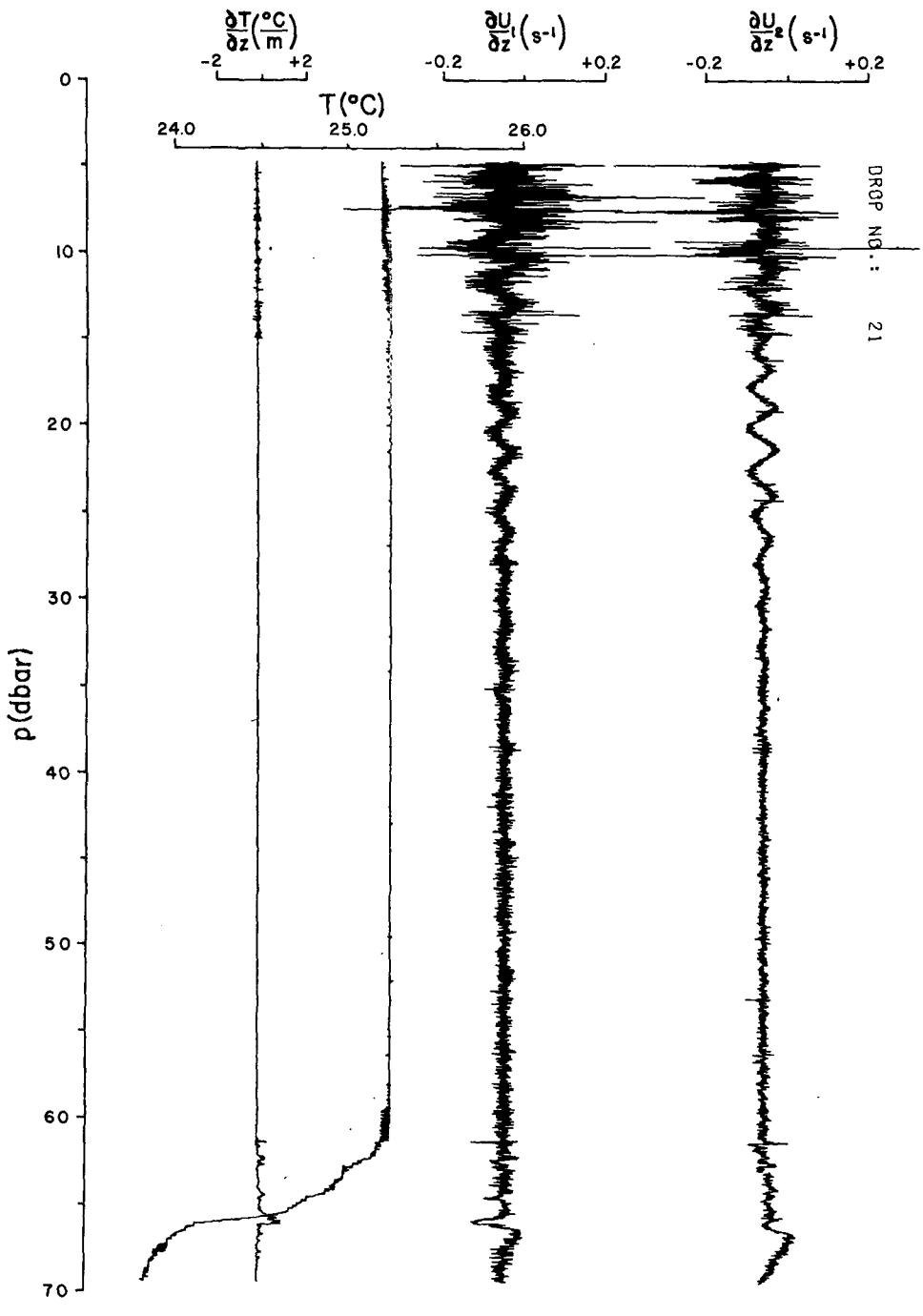

FIG. 2. CAMEL 21 profiles of temperature (T), gradient temperature ($\partial T/\partial z$), and two orthogonal components of the vertical shear of horizontal velocity ($\partial U_1/\partial z$ and $\partial U_2/\partial z$) through the surface mixed layer at a station ~60 km northeast of Bermuda. The mixed layer is quiescent below ~15 m, revealing very clearly the low-frequency oscillations, decaying with distance from the surface, which frequently contaminated near-surface dissipation measurements. As well, it is clear that, although the large fine-structure temperature gradient just below 65 m produces a transient offset in both shear traces, it does not produce high-frequency contamination which might be interpreted as turbulent velocities in the dissipation range.

ferences between the two estimates of ϵ: the profiles presented in this paper begin at a depth where the two estimates of ϵ agree to within a factor of 2.

Since computed values of ϵ vary by almost four orders of magnitude above system noise, we normally present profiles of $\log\epsilon$ with ϵ in units of cm^2 s^{-3}.

Where both shear channels are available, the lower of the two independent estimates is assumed to be least influenced by noise and plotted as a bar over the appropriate pressure range. During the first set of measurements, a grounding problem in the shear circuits caused a fairly high noise level, $\log\epsilon \approx -5$, which is used as a baseline for the bar profiles; occasional values less than this are plotted to the left of the line $\log\epsilon = -5$. This noise level was improved to $\log\epsilon \approx -5.5$ by the second observation period.

b. Velocity profiles

Numerous velocity profiles were obtained in conjunction with the dissipation profiles, with an Electromagnetic Velocity Profiler, EMVP (Sanford *et al.*, 1978a) and a similar device, the AVP (Drever and Sanford, 1976). The EMVP and AVP yielded profiles of the depth-variable currents relative to an unknown, depth-independent velocity. The purpose of the relative velocity profiles was to describe the large-scale shear structure in which CAMEL observed dissipation.

The instrumentation, principles of operation and general treatment of data for both the EMVP and AVP are described in the references above. In the present work 15 measurements of motion-induced electric fields and direction are processed to yield a velocity determination every 8 m or so. Velocity uncertainties at this vertical resolution was typically 0.5 cm^{-1} s. All EMVP and AVP profiles have been processed for velocity and water properties (temperature, temperature gradient salinity and density) at the nominal 8 m vertical spacing extending from the sea surface to bottom. Data above 50 m on the downward-measured profiles are frequently missing due to bubbles in the electrode system.

3. The first observation period: 18–23 October 1975

The first period of observations at the mid-Sargasso site included a variety of meteorological conditions, recorded in the set of standard meteorological observations taken on the ship. The values in Table A1 (see Appendix) were taken directly from the bridge log of the *Knorr*, so not to disguise the quality of the data. Wind speed and direction should be fairly accurate, since the ship was almost always stationary, while launching, recovering or waiting for profilers. Sea and swell states are subjective estimates and agree well with (equally subjective) descriptions recorded at the time of each CAMEL profile. Definitions of the Beaufort codes for wind speed, sea and swell conditions are given in Table A3. The first dissipation profile (C3) was taken after a period of strong winds (force 6–7, 11–17 m s^{-1}), in the highest sea state encountered during the cruise. The following day was one with fairly steady winds of 6–8 m s^{-1}, while passage of the front shown in the surface pressure map of Fig. 3 around 2000 GMT 20 October caused a sudden shift in wind direction, increased wind speed and an associated increase in sea state. C5 was taken about 12 h after this frontal passage, while profiles C7 and C8 were made at intervals during the following two days of decreasing wind, sea and swell. Winds had been freshening for a few hours before launch of C9 but had not yet had much effect on sea state.

The first profile, C3, was separated from the others by almost 48 h. One of the shear channels was broken during a clumsy launch, and the remaining channel had both a high noise level and severe temperature sensitivity. Nonetheless, in view of long-standing debate about the mechanism of turbulence generation in the surface mixed layer, the profile seems interesting enough to include despite its faults. Fig. 4 shows the observed dissipation and temperature profiles: the actual shear profile is included, as well as the derived dissipation plot. Derived values of ϵ are not shown below 115 db, where regions of large temperature gradient in the upper part of the seasonal thermocline produce spurious low-frequency offsets in the shear signal. The temperature sensitivity of the probe does not affect measurements within the mixed layer, which by definition does not contain large temperature gradients, nor in the 10 m thick patch of high dissipation between 102 and 112 m, since this occurs above the large finestructure gradient which marks the mixed-layer base. Near the surface is a high dissipation region, contaminated by the low-frequency periodic signal mentioned above: the low-frequency part of the signal is detectable to about 50 db, but the high-frequency turbulence signal decreases rapidly below about 20 db with many values at or near the noise level ($\log\epsilon \approx -4.6$ for the profile). Values rise again as the temperature decreases more rapidly at the base of the surface layer, where a 10 db thick patch of high dissipation is found. Thus, with surface winds of ~6–10 m s^{-1}, and sea state 5 following a period of stronger (11–17 m s^{-1}) winds, the turbulence driven directly from the surface seems to be confined to the upper 20 db of the water column, even though the underlying density stratification was very weak (a change of sigma-θ of 0.12 g ℓ^{-1} between 30 and 100 db was observed on a WHOI-Brown CTD cast following the CAMEL profile).

The following four dissipation profiles were taken at roughly 12 h intervals starting at 1400 GMT 21 October, and are shown with accompanying temperature profiles in Fig. 5. The temperature profiles are not high quality, as the thermistor carried on the CAMEL was failing through profiles C5 and C7, finally breaking entirely during launch of C8. However, over the limited pressure range shown, the

temperature profiles for C5 and C7 agree reasonably well with those taken with the WHOI-Brown CTD a few hours before or after; since the details of mixed-layer shape can change significantly over the period of a few hours, it seemed preferable to use the profiles taken at the same time as the shear profiles, whenever possible. For C8, the temperature profile was taken from an EMVP drop launched within 4 min of the CAMEL. The thermistor was replaced for C9, so this is again a simultaneous temperature profile.

The first profile of this set, C5, shows strong ($\log\epsilon \approx -3$) turbulent energy dissipation to about 100 db during the period of increased winds (force 5, 9–11 m s^{-1}) following frontal passage. Values drop to the noise level ($\log\epsilon \approx -5$) just at the base of the mixed layer then rise again in a thick (17 db) layer which is less uniform in temperature than the surface mixed layer, but still has a fairly small temperature gradient compared to the underlying seasonal thermocline, in which dissipation is sporadic and weak. By C7, the local wind had dropped to ~1.5 m s^{-1} and both sea and swell were decreasing; the region of strong and fairly uniform dissipation has decreased in thickness to ~65 db and the remainder of the mixed layer is near noise level. In this profile, the seasonal thermocline contains a number of thick patches of strong dissipation. In particular, note that the strongest (at ~160 db) is associated with the low gradient region of a large step in the temperature profile. Both profiles C8 and C9 were taken during a period of light winds (0.5–3 m s^{-1}), and low seas and swell. Both show a layer of fairly uniform dissipation, now confined to the upper 40–45 db of the SML, while the remainder of the layer contains sporadic patches, weaker by an order of magnitude. It should be emphasized that the temperature profile plotted with C8 is, in fact, from another profiler separated from CAMEL by at least a few hundred meters in horizontal distance and by 4 min in launch time. Thus the finescale temperature structure should not be related in any detail to observed patches of high dissipation. The noise level of the estimate of ϵ increases to $\sim\log\epsilon = -4.7$ for this one drop, an electronic problem associated with the thermistor failure. Profile C8 contains one or two strong dissipation events within the seasonal thermocline, while by C9 there remain only weak events with characteristically small vertical scales, often overestimated by the vertical interval of ~2.5 db used for processing the shears.

The sequence of profiles C5–C9 shows changes in SML dissipation levels which seem acceptable in the context of a model in which surface wind forcing generates turbulence throughout the mixed layer: as the winds die and seas calm, the turbulence dies away, first at the bottom of the mixed layer where work done against buoyancy forces acts as a localized

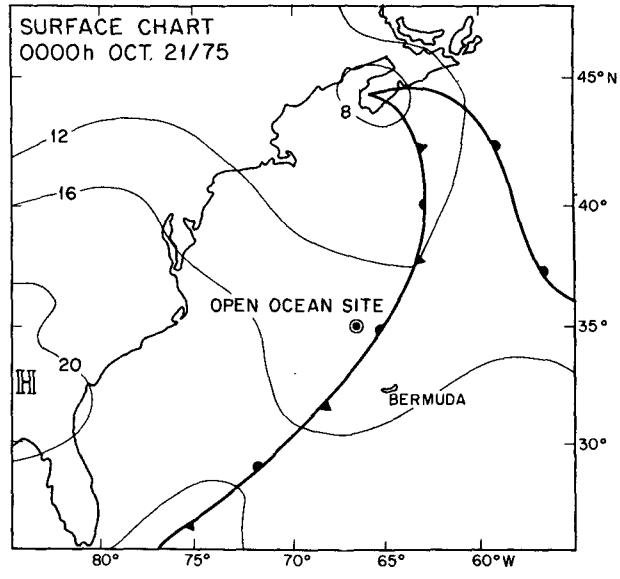

FIG. 3. Surface atmospheric pressure map showing the front which passed our observation site at approximately 2000 GMT 20 October. Contours are labeled as millibars in excess of 1000 mb.

sink of turbulent energy, and then more gradually in the rest of the well-mixed layer through the action of dissipation. The first profile, C3, does not fit comfortably into this model, however. Taken with local winds as strong as those during C5 and in considerably rougher surface wave conditions resulting from the previous period of even stronger winds, C3 shows a region of high dissipation confined to the upper 30 db of the mixed layer. This may represent some limit for turbulent dissipation driven directly by surface wind/wave processes, while the much deeper penetration evident in C5 may have been produced by the change of surface wind associated with a frontal passage, in the manner suggested by Pollard *et al.* (1973). However such a straightforward conclusion is impossible in view of the fact that the surface buoyancy fluxes, estimated roughly from the wind speeds and air-sea temperature differences reported from *Knorr* (for details of such a parameterization, see Section 5) were probably stabilizing for C3, C5 and C9 but destabilizing for C7 and C8. Certainly the variety of meteorological conditions during this first observation period makes it impossible to draw firm conclusions about mixed-layer dynamics from our restricted data set. As mentioned in the Introduction, the main reason for presenting this first set of measurements in some detail is to add to the presently sparse set of direct measurements of turbulent energy dissipation rate in the ocean SML under conditions of active wind forcing, in face of the growing number of theoretical attempts to parameterize turbulent dissipation in dynamical models of the mixed layer.

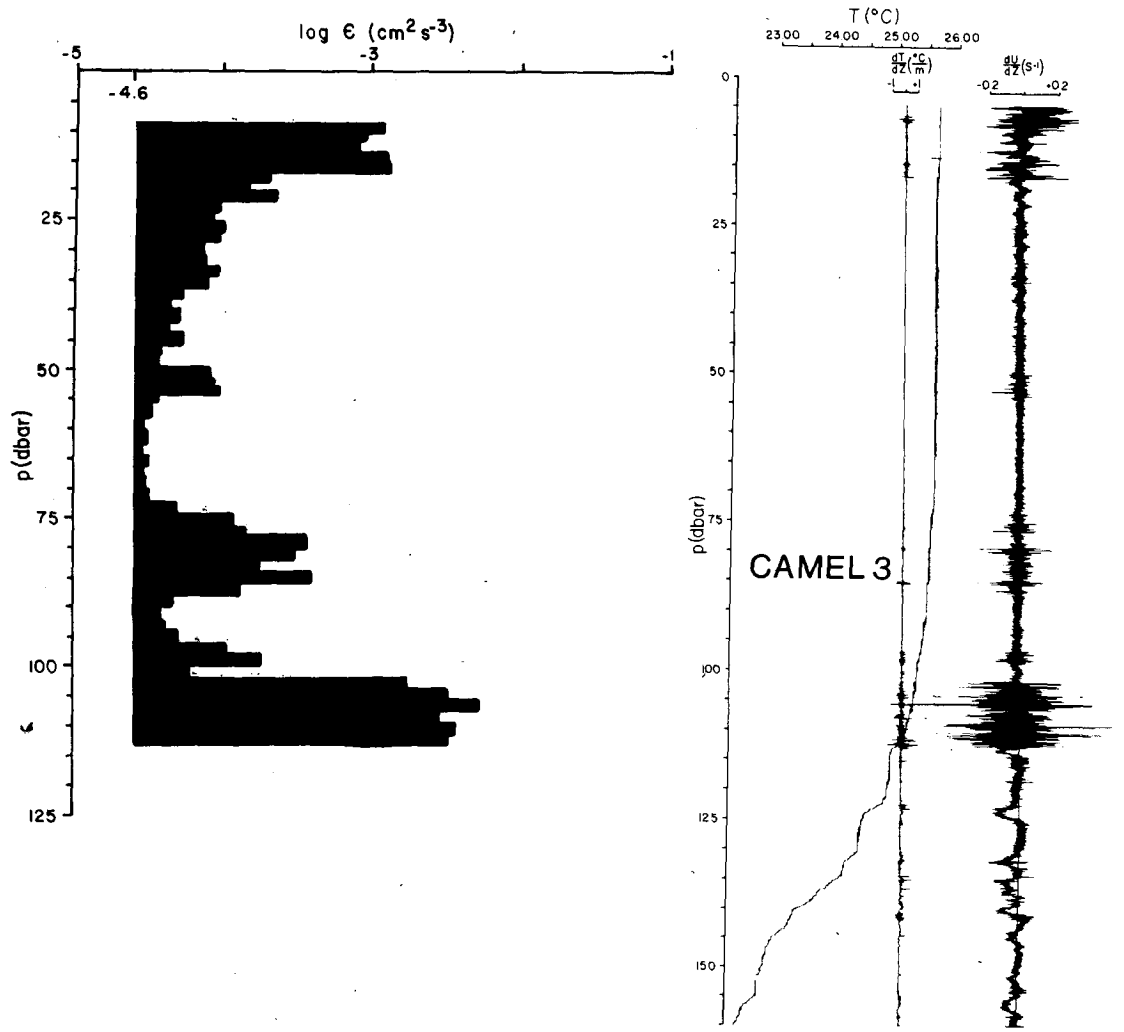

FIG. 4. Upper ocean profile of mean temperature, high-frequency gradient temperature, velocity shear and estimate of turbulent energy dissipation rate ϵ derived from shear, as measured at a site in the Sargasso Sea (35°N, 66° 30'W). Surface wave conditions were rough, with whitecapping, following the strongest winds encountered during the cruise.

The pioneering measurements made from a submarine by Grant *et al.* (1968) in 1962 have remained the only readily available values for ϵ in the ocean surface layer far from lateral boundaries. These measurements, taken under unreported surface wind conditions, showed a continuously turbulent SML. Heavily averaged values of ϵ from horizontal runs at three discrete depths ranged from 2.5×10^{-2} cm^2 s^{-3} ($\log\epsilon = -1.6$) at 15 m depth, to 2.3×10^{-3} cm^2 s^{-3} ($\log\epsilon = -2.6$) at 43 m, just above the reported mixed-layer base of ~50 m. Dissipation values measured from CAMEL in the much deeper (100–125 m) mixed layer in mid-Sargasso rarely exceed 1×10^{-2} cm^2 s^{-3} ($\log\epsilon = -2$), and often fall to the system noise level of $\sim 1 \times 10^{-5}$ cm^2 s^{-3} over a significant percentage of the layer depth. We also note that very abrupt changes in dissipation level with depth within the mixed layer seem characteristic. A particularly striking example can be seen in the mixed layer of C7, where ϵ decreases from an average of around 4×10^{-4} cm^2 s^{-3} above 70 db to the noise level over a vertical interval less than 2.5 db. A model of mixed-layer dissipation as a smoothly varying function of z, as proposed by Elsberry *et al.* (1976) or, with the addition of a constant "background" dissipation by Alexander and Kim (1976), may prove appropriate in the time-averaged sense for which it is proposed, but it is clearly insufficient as an instantaneous description of any of the observed profiles.

4. The second observation period: 7–8 November 1975

The second set of observations was taken during a period of fairly uniform light winds and calm seas, as can be seen from Table A2. The high-pressure area shown in Fig. 6, the surface pressure map for 0600 GMT 8 November, had been moving slowly across the area from the west, so that the mid-ocean site should not have experienced any pro-

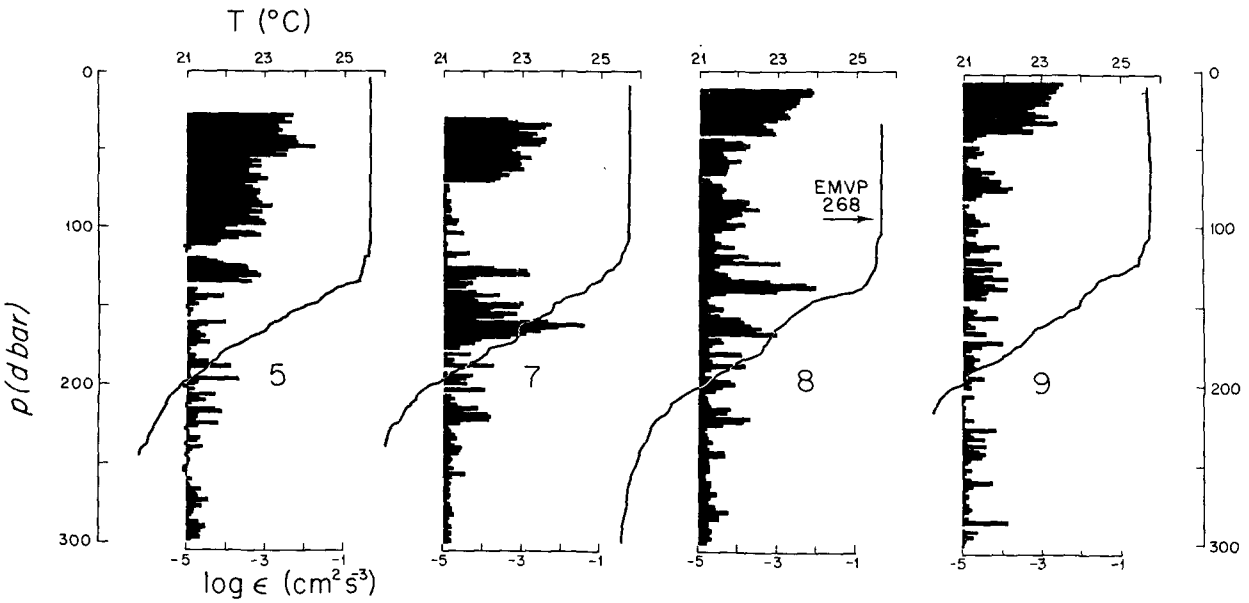

FIG. 5. Profiles of mean temperature and turbulent energy dissipation rate ϵ, taken at roughly 12 h intervals after passage of the atmospheric front shown in Fig. 3. Local wind and sea state were generally decreasing during the 2-day period.

longed periods of strong winds for at least two or three days before our arrival.

The time history of the SML depth as deduced from temperature is presented in Fig. 7, using profiles from various instruments: the CTD, Sanford's EMVP [both down (D) and up (U) profiles], and Williams' profiler SCIMP (Williams, 1974). This procedure is justified by close agreement of temperature profiles taken on other simultaneous drops of EMVP and SCIMP, and by the presence of three CTD lowerings as references within the series. At the start of observations, the surface layer was not well-mixed below 100 db. The major change occurred quite quickly, over the 7 h between EMVP 320U and CTD75, and for the rest of the time, the surface layer appeared well-mixed to about 135 db with only minor variations of thickness, which might be expected as a result of internal wave motions in the seasonal thermocline.

The change in character of the mixed layer was not confined to the temperature field. Fig. 8 is a plot of T, S and σ_t profiles from the first (74) and last (76) CTD casts, showing that salinity (hence density) also become uniform throughout the layer. We note that the peculiar structure of salinity near the base of the mixed layer in CTD 74 also appears in the salinity profile of SCIMP 15, taken at the same time as EMVP 320D, but disappeared by SCIMP 16 (Williams, personal communication). It should also be noted that the surface layer temperature increased and salinity decreased during the period of observations. The decrease of salinity in the recorded absence of local precipitation must certainly be attributed to advection. Since the change in heat content associated with the observed increase in mixed-layer temperature by ~0.1°C in one day over a depth of 135 m is roughly 1350 cal cm^{-2}, and the theoretical maximum solar input at 35°N during October–November is only about 500 cal cm^{-2} day^{-1} in the absence of an atmosphere (Hess, 1959), it can be concluded that the temperature change is also mainly an advective effect.

Mean velocity profiles were obtained from five paired drops of EMVP and AVP, spaced every 6 h. The quality of the AVP profiles increased slightly

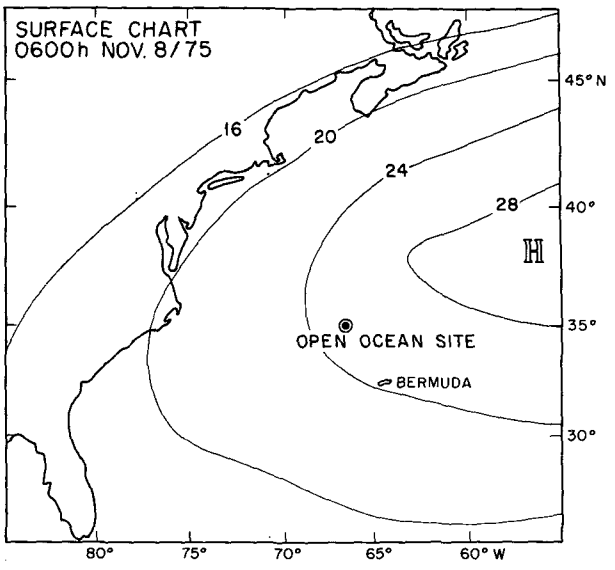

FIG. 6. Surface atmospheric pressure map at a time midway through the second set of observations at the mid-Sargasso site. The large high pressure system had been drifting slowly across the area from the west for 3 or 4 days prior to this time. Contours are mb in excess of 1000 mb.

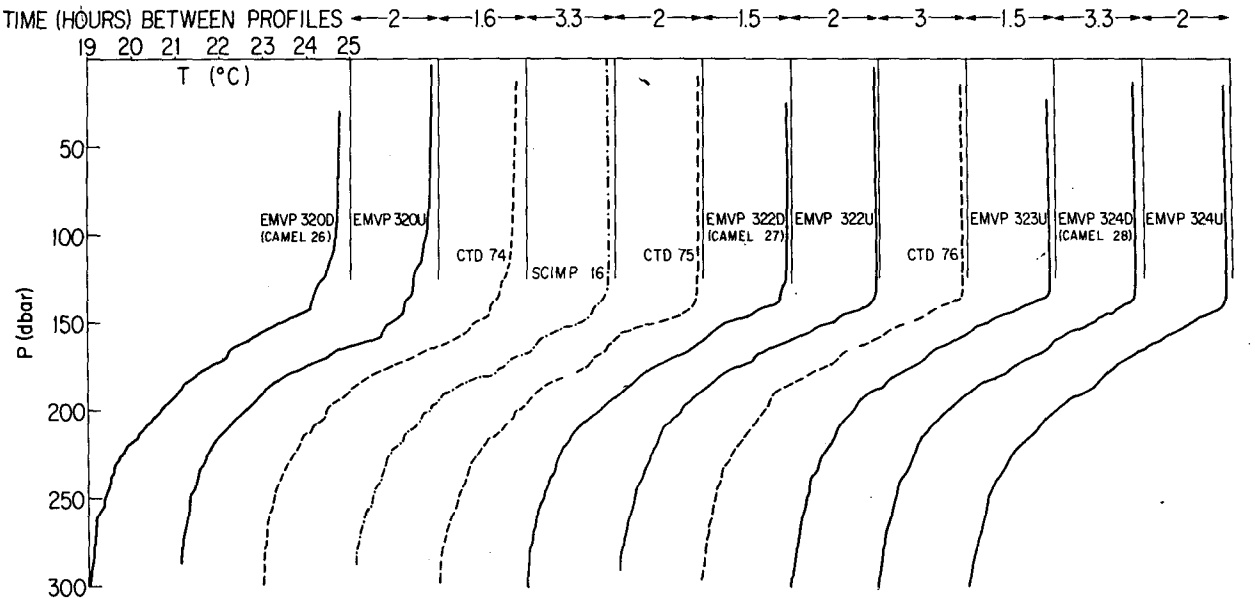

FIG. 7. Temperature profiles taken during the second occupation of the mid-Sargasso site. To obtain roughly equal time spacing between profiles, data from a number of profilers have been used. Consecutive profiles are displaced by 2°C, with 25°C marked as a vertical line from surface to 125 db.

with time as the electrodes on this new device became quieter with repeated use. The series of velocity observations, shown in Fig. 9 in terms of east and north components, has only one gap, due to an unsuccessful EMVP profile and noisy AVP measurements on drop 4D above ~700 db. Both instruments normally invert at the bottom of the ocean and provide profiles on both down and up transits. At the mid-Sargasso site, the profilers took ~1½ h to reach the bottom: thus near-surface velocity profiles shown in Fig. 9 are separated by ~3 h. Standard data quality checks result in some missing data, particularly in EMVP down profiles near the surface, due to bubbles in the electrode system. The down and up profiles of EMVP and AVP generally agree to within 1 cm s^{-1} rms between the surface and 1200 db. The exceptions, shaded in Fig. 9, are differences of up to 5 cm s^{-1} noted in SML values of the pairs 322U/5U, 323U/6U and 324D/7D (note that the surface layer comparison

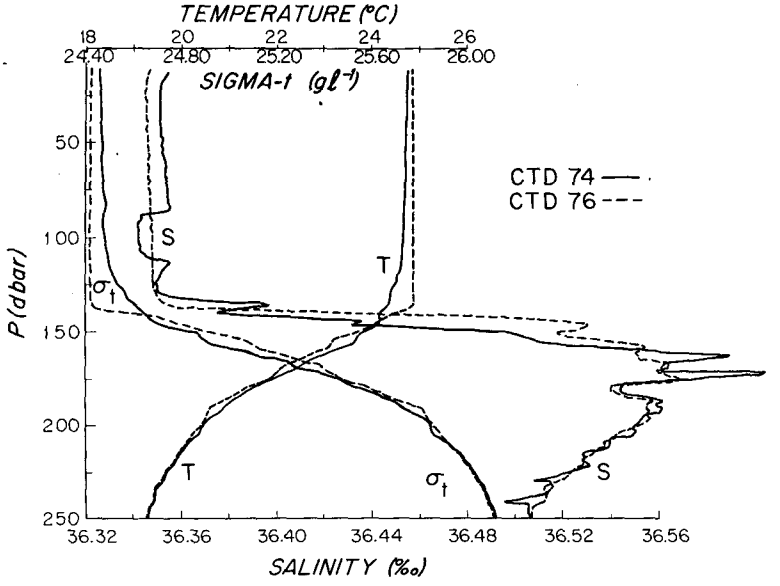

FIG. 8. Profiles of T, S and sigma-t from the first (74) and last (76) CTD casts during the second observation period. In the 12 h separating the two profiles, the surface layer became well mixed in all properties to 135 db, with accompanying increase in temperature and decrease in salinity.

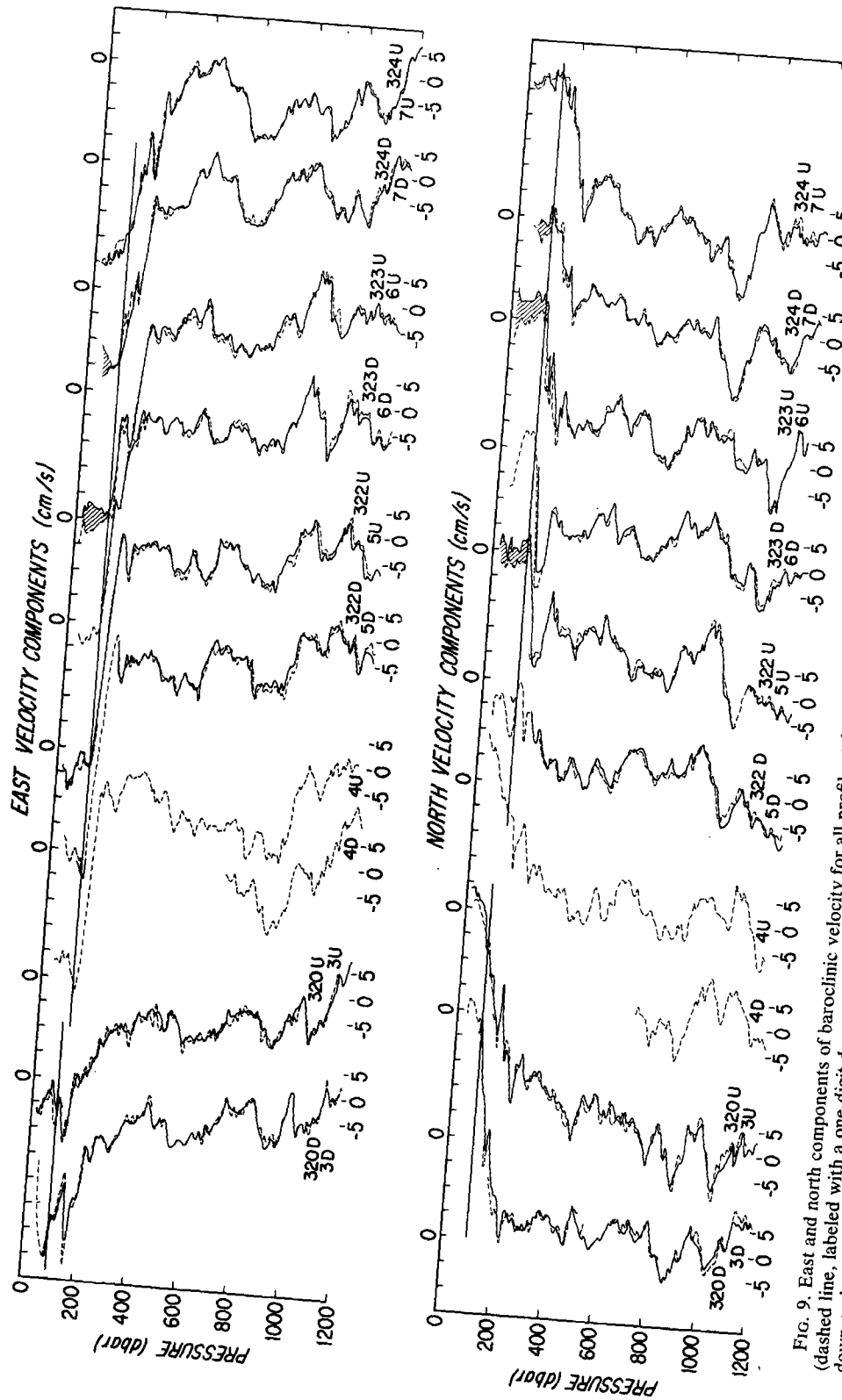

FIG. 9. East and north components of baroclinic velocity for all profiles taken by EMVP (solid line, labeled with a three-digit drop number) and AVP (dashed line, labeled with a one-digit drop number) during the second observation period at 35°N, 66° 30'W. D and U beside the drop numbers refer to down and up profiles, respectively. Horizontal lines mark the base of the mixed layer, while shaded regions emphasize nearly simultaneous profiles exhibiting unusually large differences in mixed-layer speed.

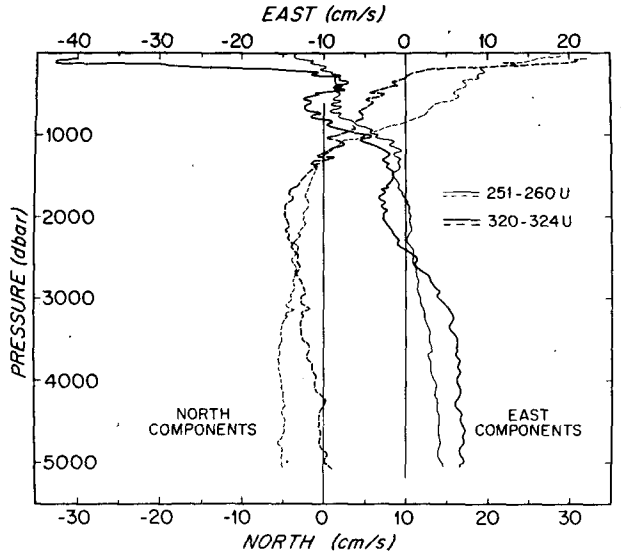

FIG. 10. Profiles of time-mean east (solid) and north (dashed) components of relative or baroclinic velocity for the entire water column. Both data sets were obtained at 35°N, 66° 30'W, with 251–260 (light lines) occurring between 19 and 21 October and 320–324 (heavy lines) on 7 and 8 November, 1975.

for 323D/6D is not available). For the pair 323U/6U, the profilers surfaced about 7 min and 100 m apart, time and space differences typical of all the EMVP/AVP paired launches. Considering the agreement elsewhere in the water column, these results indicate the presence of substantial velocity shears ($\sim 10^{-3}$ s^{-1}) in the mixed layer, varying considerably in space and/or time at a time when the SML is very well mixed indeed (CTD 76 was taken ~1½ h before 323U).

The base of the uniform temperature surface layer is marked on the velocity profiles as a horizontal line, at 100 db for the first two profiles and at 135 db for the remainder. Below this surface mixed layer, it is easy to see the now familiar mirror-imaging of velocity profiles taken half an inertial period apart in time (Leaman and Sanford, 1975); in Fig. 9, for example, drops 320D, 322D and 324D are separated by roughly half-inertial periods. This rotation of the velocity field due to largely horizontal currents associated with waves of near-inertial period is less obvious in the near-surface region, because of the presence of a large mean shear between 100 and 200 db. Averaging over one inertial period is a rough way of filtering out the high-energy inertial shears, leaving usually less energetic shears of larger vertical wavelengths. The mean profiles shown in Fig. 10 are computed by a rotary least-square fit of the up profiles in Fig. 9 (including AVP 4U) to a model consisting of two velocity contributions, a time-mean plus a component which rotates anticyclonically at the local inertial period (~21 h). The light and heavy lines in Fig. 10 show east and north components of the time-mean contribution to the flows during the first and second observation periods, respectively. For the second period, we see a strong surface layer mean flow, bounded below by a very large mean shear ($\sim 10^2$ s^{-1}) and overlying a mean shear profile notable for its deep (>1000 db) structure. The deep velocity structure observed on 320–324 is very unusual, for most mean shear profiles show little structure below the main thermocline, like the relatively featureless mean profiles of drops 251–260 below 1000 db. It seems likely that the strong near-surface motion is related to the deeper, modally richer than usual baroclinic flow. Much of the variation in shear across the base of the mixed layer observed in individual profiles in Fig. 9 is due to the superposition of vigorous inertial motions on the large mean shear. With regard to the origin of the mean velocity structure, we note that a Gulf Stream cold-core ring centered roughly at 34° 40'N, 64° 55'W was observed by Richardson (1976) on a cruise two weeks after our second set of observations (at 35° 00'N, 66° 30'W). A measurement of the absolute velocity profile through the high-velocity core of such a Gulf Stream ring, taken by Sanford *et al.* (1978b) in December 1976, shows strongly surface-intensified flow reminiscent of profiles 4D through 324U presented in Fig. 8. Thus it seems possible that the changes in density and flow fields are associated with advection of a cold-core ring in the vicinity of our measurement site. Another possibility which may be relevant to the mean flow is the suggestion of Philander (1976) that forced internal motions of subinertial frequency are strongly surface-intensified.

The timing of the dissipation profiles C26, C27 and C28 is noted in Fig. 7 relative to the time history of the vertical temperature structure. Fig. 11a shows the dissipation profiles (note the lower noise level, $\log\epsilon \approx -5.5$) and associated temperature profiles, while Fig. 11b shows in more detail the actual small-scale shear profiles through the mixed layer. A problem with the thermistor began with C28, causing the increased noise on temperature and temperature gradient signals for this drop; nevertheless, the well-mixed character of the surface layer and the very sharp temperature gradient at its base are still evident.

During this 24 h period, levels of turbulent dissipation became steadily stronger and more uniform throughout the SML. At the beginning of observations, surface layer dissipation was weak and sporadic, particularly in the region of increasing temperature gradient below 100 db, where the temperature profile was steppy, but showed little evidence of strong negative microscale gradients indicative of turbulent mixing. By the second profile, C27, the high-frequency gradient-temperature profile showed a number of patches of strong dissipative activity, both within the mixed layer and in the high-gradient region at its base. The upper

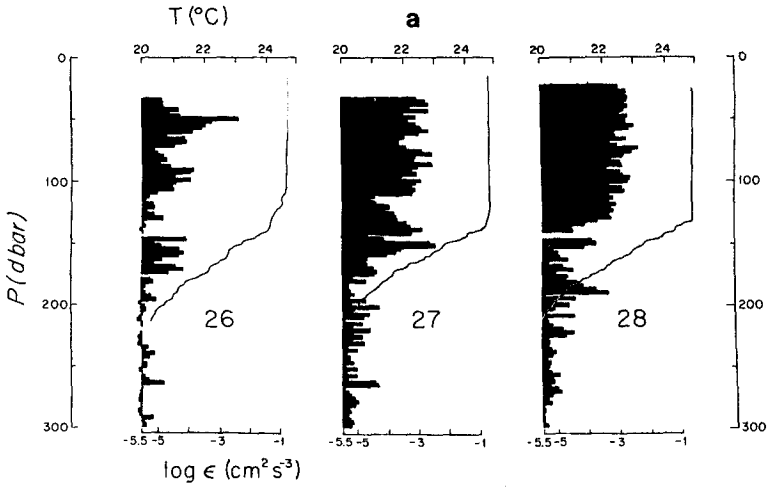

FIG. 11a. Estimates of turbulent dissipation rate calculated from measurements of small-scale shear for the three CAMEL profiles taken during development of the deep well-mixed surface layer observed by the end of the second occupation of the mid-Sargasso site.

110 db were fairly strongly turbulent, while a quieter region from 110 to 130 db lay above another (10 db) thick patch of high dissipation, just above the high mean temperature gradient region which marked the base of the mixed layer. With regard to the time scale for which such a dissipation profile may be considered valid, it is interesting to note that the same general profile, with a "gap" over roughly the same pressure interval (110–130 db), was obtained from the velocity sensors on SCIMP 16, ~3.5 h earlier than C27 (A. J. Williams, personal communication). The acoustic sensors on SCIMP measure both components of horizontal velocity with a maximum sensitivity to vertical scales of the order of 1 m, a scale closely related to the dissipation scales of 4–50 cm measured by CAMEL. By the final profile, the entire mixed layer from the surface to 135 db was strongly and quite uniformly turbulent.

The temperature gradient measurements from this CAMEL drop are not useful, but a nearly simultaneous profile from Gregg's profiler MSR showed fairly uniform levels of microscale temperature variance throughout the layer: coupled with a very low mean temperature gradient, these temperature variance measurements result in large Cox numbers, 10^3–10^6 (Gregg, personal communication).

The assumption of isotropy inherent in the estimates for ϵ gains support, for this final profile at least, from the shape of temperature and velocity spectra through the mixed layer. The temperature spectrum shown in Fig. 12 was kindly supplied by M. C. Gregg of the Applied Physics Laboratory, Seattle. Unlike most other open ocean temperature spectra, this shows about a decade of the $-5/3$ power law predicted for a passive scalar in an isotropic turbulent field. The value of ϵ deduced using k_*, the measured wavenumber at the break-in-slope of the $-5/3$ portion of this "universal" temperature spectrum, has a range of (0.64–2.4) $\times 10^{-4}$ cm^2 s^{-3} (Gregg, personal communication); the higher value uses the relation $k_*/k_s = 0.024$ (Grant *et al.*, 1968) with $\epsilon = \nu^3 k_s^4$, while the lower value uses Gibson and Swartz's (1963) laboratory value of $k_*/k_s = 1/30$. Fig. 12 also shows a "velocity" spectrum, constructed by multiplying the measured shear spectrum by the inverse of the square of radian wavenumber, which also seems to evidence nearly a decade of $-5/3$ slope on this log-log plot. The value of ϵ which results from direct integration of the measured shear spectrum, averaged over the mixed-layer depth, is (1.4–1.5) $\times 10^{-3}$ cm^2 s^{-3}, where the range comes from the two independent shear channels. For this calculation, the upper wavenumber limit k_U of the dissipation integral has been chosen to include 100% of the measured shear variance, removing the relative error inherent in the fixed integration limits normally used in profile calculations (see discussion in Section 2a.). The direct estimate of ϵ differs by a factor of 6 from the higher of the two values estimated indirectly from the temperature spectrum, reasonable agreement considering the sensitivity (through the power of 4) of the latter estimate to the experimentally determined value of k_*, the 20 min by which the temperature profile preceded the shear profile, and possible absolute errors. A Reynolds number for the layer based on $U = 0.4$ m s^{-1}, $L = 135$ m and $\nu = 10^{-6}$ m^2 s^{-1}, is $\sim 5 \times 10^7$, which may be too high for an application of Gibson's laboratory results, obtained with Reynolds numbers to only 3.8×10^4.

5. The turbulent kinetic energy balance

Present models of the surface mixed layer assume that a major part of the energy put into the turbulent

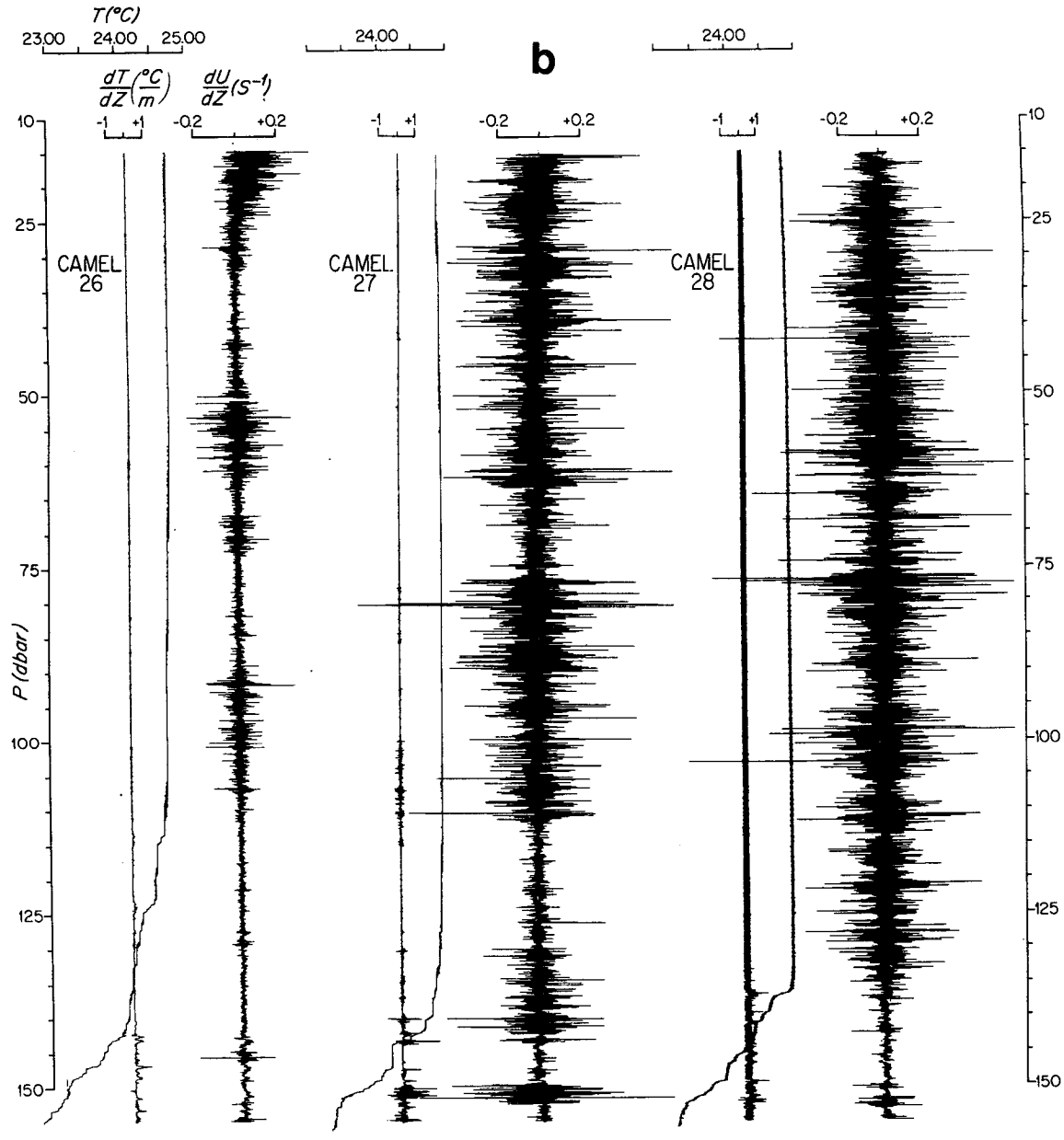

FIG. 11b. Detailed profiles of small-scale shear, mean and fluctuating temperature, through the surface layer.

kinetic energy field by various wind-wave forcing mechanisms and/or unstable surface buoyancy flux is used up by dissipation within the mixed layer, leaving only a small percentage free to deepen the layer by working against the stable buoyancy gradient at its base. Thus, our measured value of dissipation, integrated through the SML depth, should be a major component of the turbulent kinetic energy balance. It proves interesting to compare the measured magnitude of this dissipation term to magnitudes estimated for various other sources and sinks of turbulent kinetic energy, using available meteorological data and the range of standard parameterizations presently used in mixed-layer modeling. This exploration is based on the assumption that a single profile of turbulent kinetic energy dissipation can be considered valid as a time average; i.e., that repeated dissipation profiles closely spaced in time would resemble each other over times short compared to several hours, the time scale typical of changes in surface forcing. Given the apparent success of deterministic models of the mixed layer, it would be surprising if this assumption does not hold; however, we have no direct evidence to support it, since 3–4 h was the minimum time possible between profiles with the type of freely falling profiler used during FAME. A definite experimental test must await new profil-

ing techniques, but a piece of indirect evidence has already been presented in Section 4, where we noted qualitative agreement between velocity profiles, at closely related scales, of SCIMP 16 and C27 taken 3.5 h apart.

As a framework for the discussion of the turbulent kinetic energy balance, we use an integrated model of the SML (shown schematically in Fig. 13) which includes both the DKT mechanism of surface wind-wave forcing near the air-sea interface, and the PRT mechanism of mean flow shear across the base of the mixed layer. This model is the one originally formulated by Niiler (1975) and extended by Niiler and Kraus (1977) to include the effect of salinity as well as temperature on density. Density ρ_0 is assumed to be independent of depth through the mixed layer, and a linear function of z with gradient Γ below. The mean horizontal velocity $\mathbf{U}$ is assumed independent of z except in two thin boundary regions, a wave-influenced zone at the surface and a constant shear zone at the mixed-layer base, below which the ocean is assumed at rest. The kinetic energy equation for the fluctuating (zero mean) flow is

$$\frac{\partial}{\partial t}\left(\frac{\overline{c'^2}}{2}\right) = -\frac{\partial}{\partial z}\left[\overline{w'\left(\frac{p'}{\rho_0}+\frac{c'^2}{2}\right)}\right] - \overline{w'\mathbf{v}'}\cdot\frac{\partial \mathbf{U}}{\partial z} - \frac{g}{\rho_0}\overline{w'\rho'} - \epsilon, \quad (1)$$

where primes denote turbulent fields, $\overline{c'^2} = \overline{\mathbf{v}'\cdot\mathbf{v}'}$, ϵ is the rate of dissipation of turbulent kinetic energy, and the density fluctuation can be expressed in terms of temperature and salinity fluctuations as $\rho' = \rho_0(-\alpha T' + \beta S')$, where $\alpha = -\rho_0^{-1}\partial\rho/\partial T > 0$ and $\beta = \rho_0^{-1}\partial\rho/\partial S > 0$.

The first term of Eq. (1), the local rate of change of turbulent kinetic energy, is generally neglected as being at least an order of magnitude smaller than other terms in the equation (Niiler, 1975; Denman, 1973). To obtain an energy balance for the entire mixed layer, Eq. (1) is integrated from $z = 0$ to $z = -h$, a trivial operation except for the formulation of Reynolds stress $\overline{w'\mathbf{v}'}$ and turbulent density flux $\overline{w'\rho'}$ in the two boundary regions. In the upper wave-induced shear zone, the vertical fluxes of both buoyancy and momentum are taken as constant. The bottom boundary layer is considered a sink of both buoyancy and horizontal momentum; the vertical flux of horizontal momentum is used to accelerate fluid entrained from below the base of the mixed layer to the speed U of the layer, while the vertical buoyancy flux is used to decrease the density of entrained fluid to the mixed-layer density ρ_0. For the justification and mathematical formulation of these assumptions, the reader is referred to Niiler

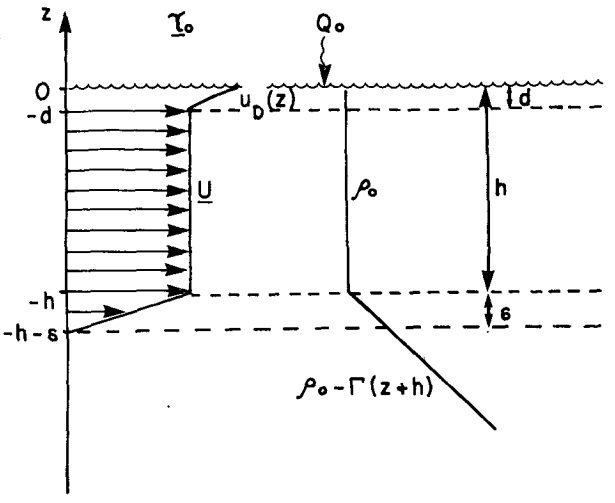

FIG. 13. Schematic diagram of the model mixed layer proposed by Niiler (1975), used as a framework for discussion of the turbulent energy balance.

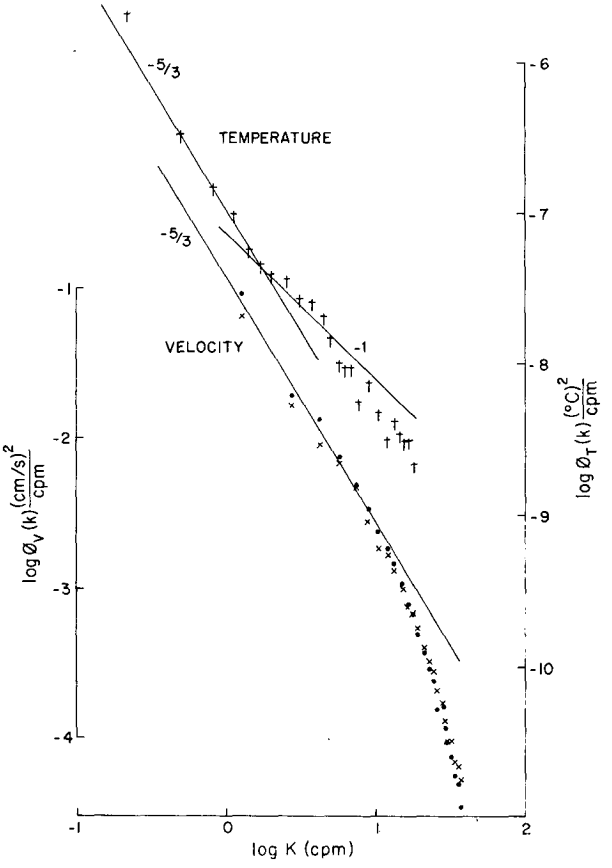

FIG. 12. Spectra of small-scale temperature and velocity through the well-mixed surface layer observed by the end of the second observation period. M. C. Gregg of the Applied Physics Laboratory kindly supplied the temperature spectrum from profile MSR 37, taken 16 min before the CAMEL profile, C28, of small-scale shear. The velocity spectrum $\phi_v(k)$ plotted here was derived from the measured shear spectrum $\phi_s(k)$ through the relationship $\phi_v(k) = k^{-2}\phi_s(k)$: spectra are shown for both shear channels. Both velocity and temperature spectra show suggestions of the classical "inertial subranges" predicted for isotropic turbulence.

TABLE 1. Parameter range for G_*, the total rate of surface mixed-layer forcing by the wind-wave field.

Source	$G_* = nu_*^3$ n	$G_* = p\tau_0 U_{10}$ p
Turner (1969)	8	*0.01*
Denman (1973)	1	*0.0012*
Halpern (1974)	3	*0.0039*
Alexander and Kim (1976)	*2.5*	0.003
Garwood (1977)	*7.6*	0.009
Richman and Garrett (1977)	17 (33–75)	*0.02 (0.04–0.09)*
Price *et al.* (1978)	*<0.15*	<0.0002

(1975); here we reproduce only the resulting vertically integrated turbulent kinetic energy equation

$$\underbrace{-\overline{w'\left(\frac{p'}{\rho_0}+\frac{c'^2}{2}\right)}\bigg|_{z=0}}_{\text{(a)}} + \underbrace{\frac{\boldsymbol{\tau}_0\cdot\mathbf{u}_D}{\rho_0}}_{\text{(b)}} + \underbrace{\frac{\mathbf{U}\cdot\mathbf{U}'}{2}\frac{\partial h}{\partial t}}_{\text{(c)}}$$

$$\underbrace{-\int_{-h}^{0}\epsilon dz}_{\text{(d)}} + \underbrace{\frac{\overline{w'p'}}{\rho_0}\bigg|_{z=h-\delta}}_{\text{(e)}} \underbrace{-\frac{g}{\rho_0}\int_{-h}^{0}\overline{\rho'w'}dz}_{\text{(f)}} = 0. \quad (2)$$

Term (a) is a source of turbulent kinetic energy associated with surface wave breaking, and is usually modeled as proportional to u_*^3 [where $u_* = (\tau_0/\rho_0)^{1/2}$ is the friction velocity in water], allowing its inclusion with the second wind-forcing source [term (b)] which arises from the interaction of the surface wind stress $\boldsymbol{\tau}_0$ with a wave-driven surface shear layer [$\mathbf{u}_D(z)$, $-d < z < 0$], and which is also normally expressed as proportional to u_*^3. This lumped parameterization of wind-wave forcing is that originally proposed (with proportionality factor $n = 1$) by Kraus and Turner (1967): since then, n has received numerous revisions. To simplify comparison, Table 1 lists various values proposed for the coefficient n in the parameterization of the combined wind-wave forcing term $G_* = nu_*^3 = [n(\rho_a/\rho_0)C_D]^{3/2}U_{10}^3$, where $u_* = (\tau_0/\rho_0)^{1/2}$ is the friction velocity in water, ρ_a (1.2×10^{-3} g cm^{-3}) air density, ρ_0(1.02 g cm^{-3}) seawater density, C_D a drag coefficient (1.3×10^{-3}), and the usual parameterization of surface wind stress $\tau_0 = \rho_a C_D U_{10}^2$ as a function of wind speed at 10 m height has been employed. Since the original references often give wind-stress forcing in terms of a fraction of $\tau_0 U_{10}$, we also give p in the expression $G_* = p\tau_0 U_{10}$, italicizing the original formulation. The values by Richman and Garrett (in parentheses) are the results of an attempt to calculate the actual transfer of momentum and energy from the wind to the ocean through the surface wave field, using approximations to the momentum transfer function based on field and laboratory experiments. These estimates are higher than the preceding number, their estimate of the total oceanic surface energy input necessary for consistency between the field observations of Denman and Miyake (1973) and the laboratory experiment of Kato and Phillips (1969) in which surface waves were absent. As a consensus of the results summarized in Table 1, a reasonable estimate of the surface wind-wave energy input to the mixed layer would seem to be 1–3% of $\tau_0 U_{10}$, though it might be expected to vary with present or absence of significant whitecapping.

The third term (c) is a source due to entrainment production as the mixed layer deepens. Pollard *et al.* (1973) considered this to be important only in the initial half-pendulum day following sudden changes in the surface wind field, but the same formulation applies when the mean shear at the base of the mixed layer is considered to be maintained by processes other than inertial motion of the surface layer.

Since $\epsilon \geq 0$ everywhere, term (d) represents a sink of turbulent kinetic energy, the loss to heat through viscosity. We are able to calculate this term directly, by summing measured values of ϵ over the mixed layer depth. The following term (e) is also a sink, representing energy loss when internal waves forced at the mixed layer base radiate away into the stratified interior of the ocean. This term has not yet been parameterized and is usually ignored; we continue this practice, remarking only that we expect it to be unimportant at times when the mixed layer is not deepening rapidly, a condition fulfilled by both of the cases we shall later discuss in detail.

The buoyancy work term (f) is more complicated to assess, as it can represent a source of turbulent kinetic energy if convective overturning due to surface cooling and/or evaporation produces more energy than is used in working against buoyancy forces during layer deepening, as fluid is entrained into the mixed layer from the stable density gradient region below; otherwise it represents a sink. If we follow Niiler (1975) in assuming that buoyancy flux to or from the ocean SML is not distributed through the layer depth but confined to the ocean surface and the SML base, then the buoyancy flux varies linearly with z from its surface value B_0 to the value B_{-h} at the mixed-layer base: $B(z) = B_0 + (B_0 - B_{-h})z/h$. This assumption is not uniformly valid, as Denman (1973) has shown that the functional dependence of solar insolation on depth should be included for wind speeds $\lesssim$6 m s^{-1}. However, neglect of this extra stabilizing heat flux will lead to an upper bound on estimates of possible destabilizing buoyancy flux. Integrating the expression for the buoyancy flux across the SML depth gives

$$-\frac{g}{\rho_0}\int_{-h}^{0}\overline{\rho'w'}dz = \tfrac{1}{2}(B_0 + B_{-h})h.$$

as an estimate for term (f). Here B_{-h} is the work done against the stable density gradient at the mixed-layer base; the magnitude of this entrainment sink

of turbulent kinetic energy is given in terms of layer depth h, rate of layer deepening $\partial h/\partial t$ and the magnitude $\Delta\rho$ of the density change between $z = -h$ and $z = -h - \delta$ by

$$B_{-h}\frac{h}{2} = \frac{-gh}{2}\frac{\Delta\rho}{\rho_0}\frac{\partial h}{\partial t} < 0$$

(for details, see Niiler, 1975). The surface buoyancy flux per unit mass can be written as

$$B_0 = \frac{-g}{\rho_0}\overline{\rho' w'}\bigg|_{z=0} = g[\alpha\overline{w'T'} - \beta\overline{w'S'}]|_{z=0},$$

where $g = 980$ cm s^{-2}, $\rho_0 = 1.02$ g cm^{-3} and the equation of state $\rho = \rho_0(1 - \alpha T + \beta S)$ is assumed, with $\alpha = 3.0 \times 10^{-4}$ (°C)$^{-1}$ and $\beta = 7.6 \times 10^{-4}$ (‰)$^{-1}$. We can estimate B_0 from standard bulk parameterizations for $\overline{w'T'}$ and $\overline{w'S'}$, given values for wind speed at 10 m (U_{10}), air temperature at 10 m (T_{10}), sea surface temperature (T_S) and relative humidity at 10 m. The first three parameters are available from the bridge log of the *Knorr*; unfortunately, wet-bulb temperature was not reported, forcing us to assume a value for relative humidity. We choose 70%, which would be an unusually low relative humidity at sea; this will if anything overestimate the latent heat flux.

The surface temperature flux $\overline{w'T'}$ is related to the total surface heat flux Q_0 by $\overline{w'T'} = -Q_0/\rho_0 C_p$, where $C_p = 0.98$ cal g^{-1} (°C)$^{-1}$ [4.1 J g^{-1} (°C)$^{-1}$] is the specific heat of sea water. Q_0 is related to its component fluxes, the shortwave radiation flux (solar insolation) $Q_I \geq 0$, the longwave radiation flux $Q_B \leq 0$, sensible heat flux Q_S, and latent heat flux Q_L by

$$Q_0 = Q_I - Q_B - Q_S - Q_L, \qquad (3)$$

where the signs of Q_S and Q_L have been chosen for the case where the ocean is losing heat to a colder overlying atmosphere.

The sensible heat flux is obtained from the parameterization suggested by Friehe and Schmitt (1976): $Q_S = \rho_a C_{pa}[A + BU_{10}(T_S - T_{10})]$, where $\rho_a = 1.2 \times 10^{-3}$ g cm^{-3} is air density, $C_{pa} = 0.24$ cal g^{-1} (°C)$^{-1}$ [1.0 J g^{-1} (°C)$^{-1}$] is the specific heat of air at constant pressure, $A = 2 \times 10^{-3}$ m s^{-1} (°C) and $B = 1 \times 10^{-3}$.

The parameterization reported by Friehe and Schmitt (1976) for water vapor flux $\overline{w'q'}$, multiplied by the latent heat of evaporation $L = 590$ cal g^{-1} (2.47×10^3 J g^{-1}), gives an estimate of latent heat flux as $Q_L = LC_q U_{10}(Q_S - Q_{10})$, where $C_q = 1.3 \times 10^{-3}$ and $(Q_S - Q_{10})$ is the difference in absolute humidity between sea surface and 10 m height. Q_S is taken as the saturated vapor pressure at the temperature of the sea surface, and Q_{10} as 70% of the saturated vapor pressure at the temperature reported at 10 m. Fortunately, the calculation of Q_L is not overly sensitive to the value chosen for the relative humidity at 10 m; our assumption of 70% relative humidity would result in an overestimation of Q_L by a factor of ~2.5 if the actual relative humidity were 100%.

The longwave radiation flux is estimated for a sky with fractional cloud cover n by the Kondratyev (1969, p. 573) formula:

$$Q_B = \delta\sigma[(T_2 + 273)^4(0.39 - C\sqrt{e_2})(1 - 0.9n) + (T_S + 273)^4 - (T_2 + 273)^4],$$

where $\delta = 0.98$ is the relative emissivity of the earth's surface, $\sigma = 1.35 \times 10^{-12}$ cal cm^{-2} K^{-4} s^{-1} (5.65×10^{-9} mW cm^{-2} K^{-4}) is the Boltzmann constant, $C = 0.05$ mm$^{-1/2}$; and T_2 and e_2 are respectively the air temperature (°C) and water vapor pressure (mm) at 2 m height, estimated from the surface and 10 m values by logarithmic interpolation.

During daylight hours, the solar shortwave radiation flux can be estimated using expressions conveniently given by Price *et al.* (1978)

$$Q_I = (RS_{\text{dir}} + RS_{\text{diff}}(1 - 0.71n)[1\text{-}RFL(\alpha)],$$

where RS_{dir} and RS_{diff} are the direct and diffuse components of the incoming radiation (functions of the sun's altitude, declination and hour angle), n is the fractional cloud cover, and $RFL(\alpha)$ is the fraction of incoming radiation which is reflected (Cox and Munk, 1956), a function of the sun's altitude.

The surface buoyancy flux also has a contribution from loss of fresh water due to evaporation, since this results in an increase of surface salinity, hence density. The buoyancy flux to the surface mixed layer associated with salt is related to fresh water flux $\overline{w'q'}$ out of the layer and mean surface layer salinity S by $w'\rho_s' = -\overline{w'q'}$ $(10^{-3} S)$ (where the factor of 10^{-3} arises through the definition of salinity as grams salt per kilogram of seawater). Using the parameterization of $\overline{w'q'}$ given in the above discussion of latent heat flux, we find that for the moderate wind speeds and air-sea temperature differences which characterize our measurements, this contribution to the surface buoyancy flux is less than one-tenth of that associated with the surface heat flux.

The sources and sinks of mixed-layer turbulent kinetic energy are summarized in Table 2, with the dual source-sink nature of the surface buoyancy flux indicated.

With the rather large time intervals between our profiles (even during the second observation period, consecutive profiles are some few hours apart), the rudimentary meteorological information available, the evidence for advection effects during the second set of observations, the lack of any parameterization for internal wave radiation, and the range of values suggested for the constant n in the usual parameterization of the surface wind-wave forcing, we do not expect to be able to use the turbulent

kinetic energy equation to predict surface layer characteristics. However, from available profiles of turbulent kinetic energy dissipation, we have selected two examples in which some subset of the source-sink terms outlined in Table 2 is absent. The magnitude of terms in the resulting simplified turbulent kinetic energy balances offer some insight into the validity of the assumptions of steady state and local balance which are fundamental to the postulated one-dimensional mixed-layer model.

a. CAMEL 21

Profile C21 shown in Fig. 2 was not taken at the mid-Sargasso site but at a location further south (32° 59′N, 64° 24′W) where the mixed layer is shallower. It is included here because of the apparent simplicity of the turbulent kinetic energy balance at the time.

C21 was taken at 2015 local time, a few hours after sunset. Wind speed was less than 1 m s^{-1} and the sea state was calm with ripples. A very low swell was present; as mentioned in Section 2, this may be the source of the periodic signal, decreasing with depth, which is apparent on both shear channels above ~30 m. The air-sea temperature difference was $T_{10} - T_s \approx -3$°C. With the exception of a near-surface region, C21 shows dissipation values at the noise level of $\epsilon \approx 5 \times 10^{-5}$ cm^2 s^{-3} right through the mixed layer and its base. The meteorological conditions, coupled with this dissipation profile allow us to demonstrate that many of the source/sink terms of Table 2 are unimportant, leaving a simple balance between convective instability and turbulent dissipation.

The quiescent nature of the dissipation profile through the mixed layer base implies that the layer is not actively deepening, so that the entrainment source and sink terms do not enter the turbulent kinetic energy balance at this time. The absence of turbulent motions at the mixed layer base also justifies neglect of the internal wave radiation sink. With no surface gravity wave breaking, one contribution to the lumped parameterization of wind-wave forcing is absent, justifying use of a moderate value of n for evaluating the remaining wind forcing source. Choosing $n = 10$ results in a value of ~0.01 cm^3 s^{-3} for this source. This proves negligible compared to the surface buoyancy flux source which has an estimated value of 2.7 cm^3 s^{-3} dominated by latent heat flux and longwave radiation flux. Thus we have only one significant source of turbulent kinetic energy, that of convective overturning driven from the top of the mixed layer as the ocean loses heat at night to an overlying cooler atmosphere. The magnitude of this source could be balanced by a uniform value of $\epsilon \approx 4 \times 10^{-4}$ cm^2 s^{-3} throughout the observed mixed layer depth of 60–70 m. Instead, the dissipation profile shows that the major part of the mixed-layer depth is quiescent, so that this input of turbulent kinetic energy must be balanced by higher values of ϵ over a smaller fraction of the mixed-layer depth, say, by $\epsilon \approx 3 \times 10^{-3}$ cm^2 s^{-3} over the upper 10 m of the water column. Since uncontaminated measurements of ϵ very near the ocean surface are probably not attainable from a vertical profiler like CAMEL, which is launched at the surface near the side of a ship, we can only say that the dissipation profile qualitatively supports the existence of higher dissipation levels in the upper 10 m and that, given the usual levels observed deeper in active mixing layers, the value of ϵ required to balance energy input is not at all unreasonable. It seems likely that at the time of C21, the turbulent

TABLE 2. Summary of source/sink terms in steady-state vertically integrated mixed-layer model.

	Term	Source (positive)	Sink (negative)
(a)	$-w'\left(\frac{p'}{\rho_0} + \frac{c'^2}{2}\right)\Big\|_{z=0}$	Surface wind-wave forcing, parameterized as nu_*^3 with $2.5 \leq n \leq 20$	
(b)	$\frac{\boldsymbol{\tau}_0 \cdot \mathbf{u}_D}{\rho_0}$		
(c)	$\frac{1}{2}\mathbf{U}\cdot\mathbf{U}\frac{\partial h}{\partial t}$	Entrainment source	
(d)	$-\int_{-h}^{0} \epsilon dz$		Viscous dissipation of turbulent kinetic energy
(e)	$\frac{\overline{w'p'}}{\rho_0}\Big\|_{z=-h-\delta}$		Internal wave radiation
(f)	$\frac{-g}{\rho_0}\int_{-h}^{0}\overline{\rho' w'}dz$	Surface buoyancy flux source ($B_0 > 0$)	Entrainment sink $\frac{gh}{2}\frac{\Delta\rho}{\rho_0}\frac{\partial h}{\partial t}$
			Surface buoyancy sink ($B_0 < 0$)

kinetic energy balance was steady and local in character, with a single surface source due to unstable convection balanced by turbulent dissipation in the upper 10–20 m of an otherwise quiescent mixed layer.

b. CAMEL 28

The second profile we choose to examine is C28, the last of the three profiles taken during the second occupation of the mid-Sargasso site, in conditions which again allow us to eliminate some sources of turbulent kinetic energy, and argue for the unimportance of others. Sea state was smooth, with ripples or wavelets (Table A2): the gravity wave breaking source was absent, allowing us to argue again for a moderate choice of $n = 10$ in the parameterization of wind-stress forcing.

Fig. 7 indicates that the SML depth is not increasing rapidly during the last 10 h of observations—the observed variations in mixed-layer depth are of the order ±5 m and could be produced solely by internal wave motions in the absence of layer deepening. With large time intervals between profiles, we cannot average out this possible effect of internal waves to arrive at a meaningful value for $\partial h/\partial t$, the rate of mixed layer deepening. However, noting that $\partial h/\partial t$ enters both entrainment source and sink terms, we examine their ratio $\gamma = U^2/(gh\,\Delta\rho/\rho_0)$. A value of 1 indicates that the energy available from the mean shear just equals that used up in work against buoyancy as the layer deepens. From CTD76 (Fig. 8) the density difference between the mixed layer base ($h \approx 135$ db) and 200 db is $\Delta\rho \approx 1.4 \times 10^{-3}$ g cm^{-3}. From EMVP profiles (322U, 323U in Fig. 9) around the time of this CTD cast, the observed value of U, taken here as the amount by which the (slab-like) mixed-layer speed exceeds that at 200 db, is of order 40 cm s^{-1}, well below the value of 130 cm s^{-1} which would be required to make $\gamma = 1$ with the above values for $\Delta\rho$ and h. This implies that if the layer were deepening at all, the process would be a substantial net sink of turbulent kinetic energy, even with the unusually large values of mean shear observed below the layer base. Values of ϵ measured by C28 are relatively uniform through the mixed layer right up to the sharp temperature gradient at its base; there is no sign, at dissipation scales at least, of a strong sink of turbulent kinetic energy localized at the mixed-layer base. On this basis, we conclude that the layer was not actively deepening at the time, and proceed to examine whether the local wind forcing and/or surface buoyancy flux are sufficient to balance the observed dissipation of 19 cm^3 s^{-3} resulting from an average value of $\bar{\epsilon} \approx 1.4 \times 10^{-3}$ cm^2 s^{-3} over a mixed-layer depth of $h \approx 135$ m (Fig. 11). Because the wind decreased and, more significantly because the sun rose (at 1130 GMT) between the times of meteorological observations 3 h before (0900 GMT) and 30 min (1300 GMT) after C28, we have estimated wind stress and buoyancy terms for both sets of reported conditions, using for U_{10} the upper limit of the reported Beaufort code at the time.

At 0900 GMT, a wind speed of 5 m s^{-1} and the choice of $n = 10$ gives the wind-stress forcing term a magnitude of ~2 cm^3 s^{-3}. The larger value of $n = 17$ suggested by Richman and Garrett (see Table 1) would increase this to ~4 cm^3 s^{-3}, still less than the surface buoyancy flux, which with the observed air-sea temperature difference of $T_{10} - T_s \approx -2$°C, acts as a turbulent kinetic energy source of magnitude ~11 cm^3 s^{-3}, dominated by contributions due to latent heat flux and longwave back radiation flux. Since there is no large discrepancy between the magnitudes of dissipation sink and combined wind stress and buoyancy source, it appears that these two source terms could maintain a fully turbulent mixing layer of depth 135 m against the turbulent dissipation measured at the time of C28.

However, by the time at which C28 was launched, the wind speed had decreased to ~3 m s^{-1}, resulting in a lower estimate of ~0.5 cm^3 s^{-3} for the wind stress forcing (or 1 cm^3 s^{-3} if we allow the higher value of $n \approx 17$). This change in source magnitude is insignificant compared to the change in surface buoyancy flux which accompanies sunrise. By very shortly after sunrise, the heat flux due to absorption of incoming shortwave radiation dominates continuing loss due to latent heat flux, and reverses the sign of the surface buoyancy flux. At the time of C28, the stabilizing buoyancy flux amounts to a sink of turbulent kinetic energy with an estimated magnitude of ~15 cm^3 s^{-3}; added to the measured dissipation sink of 19 cm^3 s^{-3}, this produces a large energy deficit in the turbulent kinetic energy balance, a deficit originating shortly after sunrise an hour previous. This conclusion can only be strengthened if, indeed, there are any losses due to layer deepening (which we assumed unimportant) and to internal wave radiation (which we are unable to assess). Thus although the dissipation profile of C28 would be compatible with a steady-state turbulent kinetic energy balance under the local meteorological conditions 3.5 h previous, it is not compatible with conditions existing during the hour preceding the profile.

It seems most likely that during the time of rapid change in surface forcing caused by sunrise, the steady-state assumption $\partial \overline{c'^2}/\partial t = 0$ is not valid and the deficit in the turbulent kinetic energy budget is being supplied by running down the turbulent velocity field. A range of 1–38 cm^2 s^{-2} can be estimated for the turbulent kinetic energy $\overline{(c'^2)}/2$ if we assume that the 1–6 cm s^{-1} horizontal velocities measured over 1–5 m scales by SCIMP16 (A. J. Williams, personal communication) are typical of the energy-containing eddies of the turbulent velocity field.

The upper limit of this range is unlikely to be exceeded, as none of the EMVP profiles show horizontal velocity fluctuations exceeding $\sim\pm 5$ cm s^{-1} within the mixed layer. Since the turbulent dissipation rate would be expected to decrease with time during decay, while the stabilizing buoyancy flux would continue to increase up to local noon, it is probably reasonable to calculate the time necessary to reduce the turbulent kinetic energy (and associated dissipation levels) to zero at the constant rate $(D + B)/h \approx 2.5 \times 10^{-3}$ cm^3 s^{-2} which combines the sinks of dissipation $D \approx 19$ cm^3 s^{-3} and stabilizing buoyancy flux $B \approx 15$ cm^3 s^{-3} typical of conditions at the time of C28. This calculation yields a range of 0.1–4 h for the decay time scale, suggesting that if the level of the rms turbulent velocity field were nearer 5 than 1 cm, its decay might be able to maintain the observed dissipation levels since the time, at sunrise, when the major source of turbulent kinetic energy was effectively shut off.

On the basis of the above analysis, it seems possible that at the time of C28 the turbulent kinetic energy balance of the surface mixed layer was local but non-steady. However, of crucial importance to this conclusion is the assumption, implicit in our calculation of an observed magnitude of turbulent dissipation, that values of ϵ in the upper 15 db of the water column, which we did not measure, are the same order of magnitude as those just below. Consider, for example, that the effect of a value of $\epsilon = 1 \times 10^{-2}$ cm^3 s^{-2} (an order of magnitude larger than the value in the rest of the mixed layer) over the top 15 db would be to double the magnitude of the dissipation sink $D = \int_{-h}^{0} \epsilon dz$. This would substantially reduce the decay time scales estimated above, and make it increasingly difficult to believe in a local, if non-steady, balance of the turbulent kinetic energy equation. If at the opposite extreme, the value of ϵ were effectively zero through the top 15 db, one might argue that the effects of the strongly stabilizing buoyancy flux were still confined near the surface, not having had sufficient time to affect the turbulent kinetic energy balance within the mixed layer proper; longer decay times result, since turbulence over most of the mixed-layer depth need be maintained only against the observed dissipation.

6. Summary and conclusions

We have presented several profiles of ϵ, the rate of dissipation of turbulent kinetic energy, through deep surface mixed layers observed during two occupations of a mid-Sargasso site, as well as one profile observed at a site further south. These profiles are associated with a variety of surface forcing conditions (stable and unstable surface buoyancy fluxes, wind speeds from 1–10 m s^{-1}, and sea states from calm to rough with whitecapping), and form an addition to existing reports of direct measurements of ϵ which may prove useful in attempts to include dissipation explicitly in surface mixed layer models.

Profiles were much too widely spaced in time to serve as an adequate description of mixed-layer behavior during the first observation period at the mid-Sargasso site. Nevertheless, one of these profiles (C3) is of qualitative interest. C3 was associated with the strongest wind-wave forcing of any of our profiles, winds 6–10 m s^{-1} and a rough whitecapping sea following the stronger winds of a frontal passage about 8 h previous, but was taken near the end of daylight hours, after several hours of a stabilizing surface buoyancy flux due to solar insolation. The dissipation profile shows large values of ϵ in a near-surface ($<$15 db) layer overlying a deeper region where ϵ values are much weaker, often near the noise level; this suggests that at this time direct surface wind-wave forcing may be effectively balanced by dissipation and stabilizing surface buoyancy flux in a near-surface layer, and thus not available for mixed-layer deepening. The 10 db thick region of high ϵ near the mixed-layer base suggests that the layer is nonetheless deepening, perhaps through the PRT instability mechanism associated with inertial wave shear across the base of the mixed layer, recently shown by Price *et al.* (1978) to be the dominant deepening mechanism on the storm time scale.

A more quantitative discussion can be produced for two other profiles, selected for characteristics of the dissipation and the surface forcing terms which allow us to argue for the absence or unimportance of various possible sources and sinks of turbulent kinetic energy. As a framework for this discussion, we use the integrated, one-dimensional, steady-state mixed-layer model originally formulated by Niiler (1975). For the first profile, C21, the turbulent kinetic energy equation indicates the possibility of a steady local balance between one source of turbulent kinetic energy, due to unstable surface buoyancy flux, and one sink, that of turbulent dissipation. For the second profile, C28, the balance is less straightforward, and implies that one of the model assumptions must be violated. Surface conditions at the time of the profile would produce a large energy deficit in the turbulent kinetic energy budget; however, conditions 3 h earlier allow an approximate balance between two sources, wind forcing and an unstable buoyancy flux, and a single sink due to dissipation. The energy deficit indicated at the time of C28 could be supplied by running down the turbulent kinetic energy field over an estimated time scale of $\sim$4 h. It could obviously be supplied in other ways, for example if the mean velocity field of the mixed layer were not slablike, or if advection or other non-local effects were actually important. However, in view of the rapid change in the surface buoyancy forcing function that occurs at sunrise an hour before C28, it seems most

likely that it is the steady-state assumption which is invalid.

However, there are two major uncertainties in the quantitative analyses we have presented of the turbulent kinetic energy budget. The first of these is the large range of uncertainty in the value which should be chosen for n in the parameterization of surface wind-wave forcing (Table 1). Combination into one parameterization of two distinct effects (surface wave breaking and wind stress/drift current interaction) which are not always present simultaneously adds to the uncertainty. The second serious problem is the lack of reliable dissipation measurements very close to the ocean surface. We have assumed that over the missing upper portion (10–15 db) of the water column, values of ϵ are approximately the same as those measured just below. In fact, this may not be a bad assumption for C21 and C28, given the low sea states at the time of both profiles. However, we do point out that abrupt changes of a factor of 10 in ϵ are not uncommon in the part of the mixed layer which was observed, and in calculating the total dissipation a level of $10\bar{\epsilon}$ through the upper 10–15 db would make this region equally as important as the remaining 100 db at a level of $\bar{\epsilon}$.

Under certain carefully selected circumstances, it might be possible to infer an appropriate value of n (and any change in n with the onset of surface wave breaking) in the surface wind-wave parameterization from the residual of a balance of source/sink terms in the turbulent kinetic energy balance. Our analysis indicates that the integrated dissipation is a significant part of this energy balance, and that the lack of measurements of ϵ in the very near-surface regions can constitute a large uncertainty in this term. Thus for surface layer measurements, it would seem advisable to develop profilers which rise through the water column and can thus measure close to the surface without the contamination associated with the surface launch of present vehicles like CAMEL. Moreover, if the time rate of change is an important part of the turbulent kinetic energy balance following abrupt changes in surface forcing, as suggested by C28, it will be necessary to profile the energy-containing range of the velocity field (as well as the dissipation range) and to do so much more frequently than is possible with present velocity profilers.

Acknowledgments. The measurements described in this paper were funded by Office of Naval Research Contracts N00014-74-C-0262 NR083-004 (Sanford) and N00014-76-6-0446 (Osborn). We would like to thank A. J. Williams and P. Hendricks for access to SCIMP data, and M. C. Gregg for making available the temperature spectrum in Fig. 11. A. Bunker very kindly supplied surface pressure maps. We are grateful for R. W. Garwood's comments on an earlier draft of this paper, which resulted in a substantial reassessment of the proposed energy balance. Helpful suggestions from K. Denman, P. Niiler, M. Gregg and S. Pond are gratefully acknowledged. A. Gargett would like to thank the Institute of Ocean Sciences, Patricia Bay for financial support, Ms. L. Beauchemin for programming support, and the Woods Hole Oceanographic Institution for hospitality during preparation of this paper.

APPENDIX

TABLE A1. *Knorr* meteorological observations, first observation period.

Date (1975)	Time (GMT)	Wind		Sea state*	Swell* and direction	Atmospheric** pressure (inches Hg)	Air temperature (°C)	Surface water temperature (°C)	Comments
		Direction	Force*						
October									
18	0000	SW	2	2	SW/2	30.18	23.3	23.3	
	0400	SSE	4	2	SW/2	30.19	25.0	23.3	
	0800	SSE	3	2	SSE/2	30.16	23.9	23.9	
	1200	SSE	3	3	SSE/2	30.17	23.9	23.9	
	1600	SSE	5	3	SSE/2	30.15	26.7	23.3	
	2000	SSE	6	3	SSE/3	30.10	26.1	23.9	
19	0000	SSE	6	4	SSE/3	30.07	20.0	24.4	
	0400	SSE	6	5	SSE/3	30.05	25.6	23.3	
	0800	SE	7	5	SSE/5	29.98	23.3	23.3	
	1200					30.00	23.3	23.3	←Approximate time of frontal passage
	1600	SW	4	5	W/4	30.03	26.7		
	2000	SW	4–5	5	W/4	30.02	26.1	24.4	←1957: Launch C3
20	0000	SW	3	2	S/4	30.02	24.4	24.4	
	0400	WSW	4	2	W/4	30.02	26.1	24.4	
	0800	WSW	4	2	W/3	29.98	24.4	23.8	
	1200	WSW	3	2	W/2	29.99	23.3	23.9	
	1600	S	3	2	W/2	29.99	25.6	23.3	
	2000	SSW	4	2	W/2	29.92	23.9	23.9	←Approximate time of frontal passage

TABLE A1.

Date (1975)	Time (GMT)	Wind: Direction	Wind: Force*	Sea state*	Swell* and direction	Atmospheric** pressure (inches Hg)	Air temperature (°C)	Surface water temperature (°C)	Comments
October									
21	0000	WSW	5	3	W/2	29.93	21.7		
	0400	WNW	3–4	2	W/2	29.96	23.3		
	0800	WNW	5	3	W/3	29.96	23.3	23.9	
	1200	WNW	5	3	WNW/3	30.00	22.2	23.9	
	1600	WNW	5	3	WNW/4	30.06	25.9		←1405: Launch C5
	2000	NW	4	3	WNW/4	30.03	21.1	23.9	
22	0000	WNW	3	3	W/4	30.05	20.0	23.4	
	0400	NW	2–3	2	W/2	30.08	23.3		
	0800	VAR	1	1	E/2	30.06	21.7	23.9	
	1200	NW	1	1	E/2	30.06	22.2	23.9	←0947: Launch C7
	1600	VAR	1–2	1	E/2	30.10	22.8	23.9	
	2000	W	1–2	1	E/2	30.07	22.2	23.9	←2208: Launch C8
23	0000	VAR	1	1	E/2	30.10	21.1	23.9	
	0400	SW	2	1	E/2	30.11	23.3	23.9	
	0800	S	2	1	E/2	30.13	22.2	23.9	
	1200	VAR	1	1	E/2	30.15	21.9	23.9	
	1600	SE	3	1	E/2	30.20	25.0	23.9	
	2000	E	3	1	E/2	30.20	23.9	23.3	←1750: Launch C9

* Beaufort codes for wind force, sea state and swell state; see Table A3.
** 1 inch Hg = 33.86 mb.

TABLE A2. *Knorr* meteorological observations, second observation period.

Date (1975)	Time (GMT)	Wind: Direction	Wind: Force*	Sea state*	Swell* and direction	Atmospheric** pressure (inches Hg)	Air temperature (°C)	Surface water temperature (°C)	Comments
November									
7	1300	ENE	1	1	NE/2	30.33	21.1	22.8	
	1700	SSE	3	1	E/2	30.34	22.2	22.8	←1609: Launch C26
	2100	SE	2	1	E/2	30.32	21.7	22.8	
8	0100	ESE	2	1	E/2	30.35	23.9	23.3	
	0500	VAR	3	1	E/2	30.35	23.9	23.3	←0230: Launch C27
	0900	SE	3	2	SE/2	30.30	21.1	23.3	
	1300	SE	2	1	SE/2	30.33	22.2	23.3	←1236: Launch C28
	1700	S	2	1	SE/2	30.29	23.3	22.8	
	2100	SSE	2	1	SE/2	30.25	23.3	24.4	

* Beaufort codes for wind force, sea state and swell state; see Table A3.
** 1 inch Hg = 33.86 mb.

TABLE A3. Beaufort codes.*

Code	Wind force code: Description	Wind force code: Wind speed ($m\ s^{-1}$)	Sea state code: Description	Sea state code: Height (m)	Swell condition code: Description	Swell condition code: Height (m)
0	Calm	<0.5	Calm–glassy	0	No swell	0
1	Light air	0.5–1.0	Calm–ripples	0–0.1	Low swell	0.3–2
2	Light breeze	1.0–3.0	Smooth–wavelets	0.1–0.5		
3	Gentle breeze	3.0–5.1	Slight	0.5–1.25	Moderate swell	2–4
4	Moderate breeze	5.1–8.2	Moderate	1.25–2.5		
5	Fresh breeze	8.2–10.8	Rough	2.5–4.0		
6	Strong breeze	10.8–13.9				
7	Moderate gale	13.9–17.0				

* *Instruction Manual for Obtaining Oceanographic Data*, 3rd. ed., 1968: U.S. Naval Oceanographic Office Publ. HOP 607, 201 pp. [NTIS AD 672850].

REFERENCES

Alexander, R. C., and J.-W. Kim, 1976: Diagnostic model study of mixed-layer depths in the summer North Pacific. *J. Phys. Oceanogr.*, **6**, 293–298.

Cox, C., and W. Munk, 1956: Slopes of the sea surface deduced from photographs of sun glitter. *Bull. Scripps Inst. Oceanogr.*, **6**, 401–488.

Crawford, W. R., 1976: Turbulent energy dissipation in the Atlantic Equatorial Undercurrent. Ph.D. thesis, University of British Columbia, Vancouver, 150 pp.

——, and T. R. Osborn, 1979: Microstructure measurements in the Atlantic Equatorial Undercurrent during GATE. *Deep Sea Res.*, **26** (GATE Suppl. II), 285–308.

Denman, K. L., 1973: A time-dependent model of the upper ocean. *J. Phys. Oceanogr.*, **3**, 173–184.

——, and M. Miyake, 1973: Upper layer modification at Ocean Station PAPA: Observations and simulation. *J. Phys. Oceanogr.*, **3**, 185–196.

Drever, R. G., and T. B. Sanford, 1976: A velocity profiler based on acoustic Doppler principles. WHOI Ref. 76–96, 43 pp.

Elsberry, R. L., T. S. Fraim and R. N. Trapnell, Jr., 1976: A mixed layer model of the oceanic thermal response to hurricanes. *J. Geophys. Res.*, **81**, 1153–1162.

Friehe, C., and K. F. Schmitt, 1976: Parameterizations of air-sea interface fluxes of sensible heat and moisture by bulk aerodynamic formulas. *J. Phys. Oceanogr.*, **6**, 801–809.

Garwood, R. W. Jr., 1977: An oceanic mixed layer model capable of simulating cyclic states. *J. Phys. Oceanogr.*, **7**, 455–468.

Gibson, C. H., and W. H. Schwartz, 1963: The universal equilibrium spectra of turbulent velocity and scalar fields. *J. Fluid Mech.*, **16**, 365–384.

Grant, H. L., A. Moilliett and W. M. Vogel, 1968: Some observations of the occurrence of turbulence in and above the thermocline. *J. Fluid Mech.*, **34**, 443–448.

Halpern, D., 1974: Observations of the deepening of the wind-mixed layer in the northeast Pacific Ocean. *J. Phys. Oceanogr.*, **4**, 454–466.

Hess, S. L., 1959: *Introduction to Theoretical Meteorology*. Henry Holt and Co., 362 pp.

Kato, H., and O. M. Phillips, 1969: On the penetration of a turbulent layer into stratified fluid. *J. Fluid Mech.*, **37**, 643–655.

Kondratyev, K., 1969: *Radiation in the Atmosphere. International Geophysics Series*, Vol. 12, Academic Press, 912 pp.

Kraus, E. B., and J. S. Turner, 1967: A one-dimensional model of the seasonal thermocline, Part II. *Tellus*, **19**, 98–105.

Leaman, K. D., and T. B. Sanford, 1975: Vertical energy propagation of inertial waves: a vector spectral analysis of velocity profiles. *J. Geophys. Res.*, **80**, 1975–1978.

Mellor, G. L., and P. A. Durbin, 1975: The structure and dynamics of the ocean surface mixed layer. *J. Phys. Oceanogr.*, **5**, 718–728.

Miyake, Y., and M. Koizumi, 1948: The measurement of the viscosity coefficient of seawater. *J. Mar. Res.*, **7**, 63–66.

Niiler, P. P., 1975: Deepening of the wind-mixed layer. *J. Mar. Res.*, **33**, 405–422.

——, and E. B. Kraus, 1977: One-dimensional models of the upper ocean. *Modelling and Prediction of the Upper Layers of the Ocean*, E. B. Kraus, Ed., Pergamon Press, 143–172.

Osborn, T. R., 1977: The design and performance of free-fall microstructure instruments at the Institute of Oceanography, University of British Columbia. IOUBC Ms. Rep. No. 30, Institute of Oceanography, University of British Columbia, 37 pp.

——, 1978: Measurements of energy dissipation adjacent to an island. *J. Geophys. Res.*, **83**, 2939–2957.

——, and W. R. Crawford, 1977: Turbulent velocity measurements with an airfoil probe. IOUBC Ms. Rep. No. 31, Institute of Oceanography, University of British Columbia, 39 pp.

——, and T. E. Siddon, 1975: Oceanic shear measurement using the airfoil probe. *Proc. Third Biennial Symposium on Turbulence in Liquids*, Rolla, Michigan.

Philander, G., 1976: Forced oceanic waves. *Ocean Modelling Newsletter*, No. 1, October 1976, Dept. of Appl. Math. and Theoretical Phys., Cambridge, U.K.

Pollard, R. T., 1970: On the generation by winds of inertial waves in the ocean. *Deep-Sea Res.*, **17**, p. 795–812.

——, and R. C. Millard, Jr., 1970: Comparison between observed and simulated wind-generated inertial oscillations. *Deep-Sea Res.*, **17**, 813–821.

——, P. B. Rhines and R. O. R. Y. Thompson, 1973: The deepening of the wind-mixed layer. *J. Geophys. Fluid Dyn.*, **3**, 381–404.

Price, J. F., C. N. K. Mooers and J. C. Van Leer: 1978 Observation and simulation of storm-induced mixed-layer deepening. *J. Phys. Oceanogr.*, **8**, 582–599.

Richardson, P., 1976: Rings and ridges. *Polymode News*, No. 8, May 1976. Woods Hole Oceanographic Institution.

Richman, J., and C. Garrett, 1977: The transfer of energy and momentum by the wind to the surface mixed layer. *J. Phys. Oceanogr.*, **7**, 876–881.

Sanford, T. B., and N. G. Hogg, 1977: The North Atlantic Fine and Microstructure Cruise, *KNORR* 52 and *EASTWARD* 75-12. WHOI Ref. 77-11, 88 pp.

——, R. G. Drever and J. H. Dunlap, 1978a: A velocity profiler based on the principles of geomagnetic induction. *Deep-Sea Res.*, **25**, 183–210.

——, —— and ——, 1978b: Mobile deep water velocity profiling in the local dynamics experiment. *Polymode News*, No. 44, March 1978, Woods Hole Oceanographic Institution.

Thompson, R. O. R. Y., 1976: Climatological numerical models of the surface mixed layer in the ocean. *J. Phys. Oceanogr.*, **6**, 496–503.

Turner, J. S., 1969: A note on wind mixing at the seasonal thermocline. *Deep-Sea Res.*, **16** (Suppl.), 297–300.

Williams, A. J., 1974: Free-sinking temperature and salinity profiler for ocean microstructure studies. *Ocean 74*, Vol. II, IEEE 74, CH0873-0-0CC, 263–269.